R. & M. No. 3523

MINISTRY OF TECHNOLOGY

AERONAUTICAL RESEARCH COUNCIL
REPORTS AND MEMORANDA

Calculation Methods for Three-dimensional Turbulent Boundary Layers

By P. D. Smith, Ph.D.

LONDON: HER MAJESTY'S STATIONERY OFFICE
1968
PRICE 19*s.* 0*d.* NET

Calculation Methods for Three-dimensional Turbulent Boundary Layers

By P. D. Smith, Ph.D.

Reports and Memoranda No. 3523*
December, 1966

Summary.

Five methods for the approximate solution of the momentum integral equations for the three-dimensional turbulent boundary layer are presented. These include the removal of the usual small cross-flow velocity restriction and the development of the streamwise shape parameter is calculated by means of an extension of Head's[1] entrainment hypothesis. The predictions of these theories and of those of a method due to Cooke[2] are then compared with the results of a series of experiments with an apparatus designed to simulate the case of an infinite yawed wing. A considerable discrepancy is shown to exist between theory and experiment which is attributed either to the streamwise skin friction being inadequately represented by an expression derived from two-dimensional flow or possibly, if less likely, to the neglect of certain terms in the derivation of the streamwise momentum-integral equation.

LIST OF CONTENTS

*Replaces A.R.C. 28 586.

This work was submitted in part fulfilment of the requirements for the degree of Ph.D. to the University of London, November 1965.

---

1. *Introduction.*

Three-dimensional turbulent boundary layers are, in all probability, the most commonly occurring form of boundary layers. Nevertheless the methods available for calculating the development of these layers are very few and until the work of the present author had been undertaken none had been compared to any extent with experiment. These methods were also in general characterised by the neglect of terms due to cross-flow in the boundary layer and the assumption that the streamwise shape parameter was a constant. The methods presented here represent an attempt to develop calculation methods to include these cross-flow terms and to calculate simultaneously the development of the streamwise shape parameter. The predictions of these methods are then compared with the results of a series of experiments which produced three-dimensional turbulent boundary layers upon an apparatus which simulated an infinite yawed wing.

The main results of this comparison between theory and experiment are that, although the cross-flow terms would appear to be adequately allowed for by the theories developed here, there still exists a considerable disparity between theory and experiment. This is attributed either to the streamwise skin friction being inadequately represented by any of the usual expressions taken from two-dimensional flow or possibly, if less likely, to the neglect of certain terms in the derivation of the streamwise momentum-integral equation.

The method of shape-factor prediction involved is an extension of Head's[1] entrainment hypothesis to the three-dimensional case and is shown here to give fair agreement with experiment.†

2. *The Boundary Layer and Momentum-Integral Equations.*

A system of orthogonal curvilinear co-ordinates (ξ, η, ζ) is used. The surface on which the boundary layer lies is denoted by $\zeta = 0$ and ζ measures the distance from the surface along a normal. On the surface $\zeta = 0$ are two families of co-ordinate curves ξ = constant and η = constant orthogonal to one another. In this system an element of length (ds) within the boundary layer is given by

$$ds^2 = h_1^2\, d\xi^2 + h_2^2\, d\eta^2 + d\zeta^2$$

---

†Since this work was completed the author has been informed that this extension has been also derived independently by Cumpsty and Head.

where h_1 and h_2 are length parameters which may be taken as functions of ξ and η only provided that the surface curvature does not change abruptly and that the boundary-layer thickness is small compared with the principal radii of curvature of the surface.

In this co-ordinate system the boundary layer and continuity equations as given by Cooke[2] for incompressible flow are:

$$\frac{u}{h_1}\frac{\partial u}{\partial \xi}+\frac{v}{h_2}\frac{\partial u}{\partial \eta}+\frac{w\,\partial u}{\partial \zeta}-k_2 uv+k_1 v^2 = -\frac{1}{\rho h_1}\frac{\partial P}{\partial \xi}+\frac{1}{\rho}\frac{\partial}{\partial \zeta}\left[\mu\frac{\partial u}{\partial \zeta}-\rho\,\overline{(u'w')}\right] \tag{2.1}$$

$$\frac{u}{h_1}\frac{\partial v}{\partial \xi}+\frac{v}{h_2}\frac{\partial v}{\partial \eta}+\frac{w\,\partial v}{\partial \zeta}-k_1 uv+k_2 u^2 = -\frac{1}{\rho h_2}\frac{\partial P}{\partial \eta}+\frac{1}{\rho}\frac{\partial}{\partial \zeta}\left[\mu\frac{\partial v}{\partial \zeta}-\rho\,\overline{(v'w')}\right] \tag{2.2}$$

$$0 = \frac{\partial P}{\partial \zeta} \tag{2.3}$$

$$\frac{\partial}{\partial \xi}(\rho h_2 u)+\frac{\partial}{\partial \eta}(\rho h_1 v)+\frac{\partial}{\partial \zeta}(\rho h_1 h_2 w) = 0\,. \tag{2.4}$$

The velocity components in the ξ, η and ζ directions are given by $u+u'$, $v+v'$, $w+w'$ where u and u' are mean and fluctuating parts respectively. The mean of a product $f'g'$ is denoted by $\overline{(f'g')}$. P is the pressure, ρ the density, μ the viscosity and k_1, k_2 are the geodesic curvatures of the curves ξ = constant, η = constant respectively, i.e.

$$k_1 = -\frac{1}{h_1 h_2}\frac{\partial h_2}{\partial \xi},\quad k_2 = -\frac{1}{h_1 h_2}\frac{\partial h_1}{\partial \eta}$$

The last terms on the right-hand side of 2.1 and 2.2 consist of derivatives of shear stress terms $\mu(\partial u/\partial\zeta)$ and $\mu(\partial v/\partial\zeta)$ together with Reynolds stresses $-\rho\,\overline{(u'w')}$ and $-\rho\,\overline{(v'w')}$. We write $\tau_1 = \mu\dfrac{\partial u}{\partial \zeta}-\rho\,\overline{(u'w)}$, $\tau_2 = \mu\dfrac{\partial v}{\partial \zeta}-\rho\,\overline{(v'w')}$ and denote their values on the surface by τ_{01} and τ_{02}.

The values of $\partial P/\partial\xi$ and $\partial P/\partial\eta$ are obtained from the flow at the edge of the boundary layer, i.e.

$$\frac{u_e}{h_1}\frac{\partial u_e}{\partial \xi}+\frac{v_e}{h_2}\frac{\partial u_e}{\partial \eta}-k_2 u_e v_e+k_1 v_e^2 = -\frac{1}{\rho h_1}\frac{\partial P}{\partial \xi} \tag{2.5}$$

$$\frac{u_e}{h_1}\frac{\partial v_e}{\partial \xi}+\frac{v_e}{h_2}\frac{\partial v_e}{\partial \eta}-k_1 u_e v_e+k_2 u_e^2 = -\frac{1}{\rho h_2}\frac{\partial P}{\partial \eta} \tag{2.6}$$

We may integrate equations 2.1 and 2.2 term by term across the boundary layer using equation 2.4 to eliminate w and equations 2.5 and 2.6 to eliminate P. We then obtain momentum integral equations and if we put these into streamline co-ordinates so that $v_e = 0$ and assume the external flow to be irrotational so that we may put $h_1 = 1/u_e$ the momentum-integral equations then become

$$\frac{\partial \theta_{11}}{\partial \xi}+\frac{1}{u_e h_2}\frac{\partial}{\partial \eta}(\theta_{12})+\frac{1}{u_e}\frac{\partial u_e}{\partial \xi}(2\theta_{11}+\delta_1)-\frac{1}{u_e}k_1(\theta_{11}-\theta_{22}) = \frac{\tau_{01}}{\rho u_e^3} \tag{2.7}$$

$$\frac{\partial \theta_{21}}{\partial \xi}+\frac{1}{u_e h_2}\frac{\partial(\theta_{22})}{\partial \eta}+\frac{2}{u_e}\frac{\partial u_e}{\partial \xi}\theta_{21}+\frac{1}{h_2 u_e^2}\frac{\partial u_e}{\partial \eta}(\theta_{11}+\theta_{22}+\delta_1)-\frac{2}{u_e}k_1\theta_{21} = \frac{\tau_{02}}{\rho u_e^3}\,. \tag{2.8}$$

An axially symmetric analogy is found by assuming the cross-flow velocity (i.e. v) and its derivatives in the η direction to be small. With this assumption and writing $(1/h_1)(\partial/\partial\xi) = \partial/\partial s$ and $h_2 = r$ so that $k_1 = -\frac{1}{r}\frac{\partial r}{\partial s}$ the momentum integral equations take the form

$$\frac{\partial\theta_{11}}{\partial s}+\theta_{11}\left[(H+2)\frac{1}{u_e}\frac{\partial u_e}{\partial s}+\frac{1}{r}\frac{\partial r}{\partial s}\right] = \frac{\tau_{01}}{\rho u_e^2} \tag{2.9}$$

$$\frac{\partial\theta_{21}}{\partial s}+2\theta_{21}\left[\frac{1}{u_e}\frac{\partial u_e}{\partial s}+\frac{1}{r}\frac{\partial r}{\partial s}\right]+\frac{1}{u_e r}\frac{\partial u_e}{\partial\eta}(\theta_{11}+\delta_1) = \frac{\tau_{02}}{\rho u_e^2}. \tag{2.10}$$

The various momentum and displacement thicknesses are defined as

$$\begin{gathered}\delta_1 = \int_0^\delta 1-\frac{u}{u_e}d\zeta\,,\ \delta_2 = -\int_0^\delta \frac{v}{u_e}d\zeta\,,\ \theta_{11} = \int_0^\delta\left(1-\frac{u}{u_e}\right)\frac{u}{u_e}d\zeta\,,\\ \theta_{12}\int_0^\delta\left(1-\frac{u}{u_e}\right)\frac{v}{u_e}d\zeta\,,\ \theta_{21} = -\int_0^\delta\frac{uv}{u_e^2}d\zeta\,,\ \theta_{22} = -\int_0^\delta\frac{v^2}{u_e^2}d\zeta\,,\end{gathered} \tag{2.11}$$

and $H = \delta_1/\theta_{11}$.

3. *The Assumed Velocity Profiles and Wall-Friction Values.*

The various suggestions for the form of the velocity profiles have been comprehensively reviewed by Cooke[2] and it is intended here only to mention those which are necessary for the calculation methods of Section 5. Since the streamwise velocity profiles in three-dimensional flow are similar to those in two-dimensional boundary layers, it has usually been assumed that the streamwise velocity profile follows a power law of the form

$$u/u_e = (\zeta/\delta)^n \tag{3.1}$$

and substitution of this into the definition of H the streamwise shape parameter yields

$$n = \frac{H-1}{2} \text{ so that } u/u_e = \left(\frac{\zeta}{\delta}\right)^{\frac{H-1}{2}} \tag{3.2}$$

The form assumed for the cross-flow velocity profile is usually

$$\frac{v}{u_e} = \left(1-\frac{\zeta}{\delta}\right)^2\frac{u}{u_e}\alpha \tag{3.3}$$

with $\alpha = \tan\beta = \tau_{02}/\tau_{01}$ where β is the angle between the direction of a streamline in the free stream and the corresponding limiting streamline on the surface of the body.

Eichelbrenner[3] has suggested that v/u_e should be written as a quintic in u/u_e,

$$\frac{v}{u_e} = \alpha_1\frac{u}{u_e}+\alpha_2\left(\frac{u}{u_e}\right)^2+\alpha_3\left(\frac{u}{u_e}\right)^3+\alpha_4\left(\frac{u}{u_e}\right)^4+\alpha_5\left(\frac{u}{u_e}\right)^5,$$

he then defines

$$\alpha = \underset{u/u_e \to 0}{\text{Lim}} \frac{v}{u} \qquad c = \underset{u/u_e \to 1}{\text{Lim}} \frac{v}{(u-u_e)}.$$

If one assumes that v/u_e is to be linear with respect to u/u_e at $u/u_e = 0$ and 1, i.e.

$$\left(\frac{\partial^2 v/u_e}{\partial (u/u_e)^2}\right)_0 = 0, \qquad \left(\frac{\partial^2 v/u_e}{\partial (u/u_e)^2}\right)_1 = 0, \qquad \left(\frac{\partial v/u_e}{\partial u/u_e}\right)_0 = \alpha, \qquad \left(\frac{\partial v/u_e}{\partial u/u_e}\right)_1 = c,$$

then applying the further boundary condition $(v/u_e)_1 = 0$ one obtains

$$\frac{v}{u_e} = \alpha\left[\frac{u}{u_e} - 6\left(\frac{u}{u_e}\right)^3 + 8\left(\frac{u}{u_e}\right)^4 - 3\left(\frac{u}{u_e}\right)^5\right] - c\left[4\left(\frac{u}{u_e}\right)^3 - 7\left(\frac{u}{u_e}\right)^4 + 3\left(\frac{u}{u_e}\right)^5\right]. \tag{3.4}$$

Unfortunately the assumed boundary condition $\left(\dfrac{\partial^2 \dfrac{v}{u_e}}{\partial (u/u_e)^2}\right) = 0$ is suspect since we may write

$$\frac{\partial^2 (v/u_e)}{\partial \zeta^2} = \frac{\partial (v/u_e)}{\partial (u/u_e)} \frac{\partial^2 (u/u_e)}{\partial \zeta^2} + \left[\frac{\partial (u/u_e)}{\partial \zeta}\right]^2 \left[\frac{\partial^2 (v/u_e)}{\partial (u/u_e)^2}\right]. \tag{3.5}$$

which at the wall with the above boundary conditions reduces to

$$\left[\frac{\partial^2 (v/u_e)}{\partial \zeta^2}\right]_0 = \alpha \left[\frac{\partial^2 (u/u_e)}{\partial \zeta^2}\right]_0.$$

But at the wall the boundary layer equations 2.1 and 2.2 give

$$\mu \frac{\partial^2 v}{\partial \zeta^2} = \frac{1}{h_2} \frac{\partial P}{\partial \eta}, \qquad \mu \frac{\partial^2 u}{\partial \zeta^2} = \frac{1}{h} \frac{\partial P}{\partial \xi}$$

therefore

$$\alpha = \frac{1}{h_2} \frac{\partial P}{\partial \eta} \Big/ \frac{1}{h_1} \frac{\partial P}{\partial \xi}$$

i.e. the limiting streamline is normal to the isobar. This implication, which may also be deduced for the triangular profile suggested by Johnston[4] is in direct contradiction with all the experimental evidence so far produced.

To overcome this we assume here a quartic in u/u_e for v/u_e and only apply the four boundary conditions

$$\left(\frac{v}{u_e}\right)_1 = 0, \qquad \left[\frac{\partial^2 (v/u_e)}{\partial (u/u_e)^2}\right]_1 = 0, \qquad \left[\frac{\partial (v/u_e)}{\partial (u/u_e)}\right]_0 = \alpha \text{ and } \left[\frac{\partial (v/u_e)}{\partial (u/u_e)}\right]_1 = c.$$

This gives

$$\frac{v}{u_e} = \alpha\left[\frac{u}{u_e} - 3\left(\frac{u}{u_e}\right)^2 + 3\left(\frac{u}{u_e}\right)^3 - \left(\frac{u}{u_e}\right)^4\right] - c\left[3\left(\frac{u}{u_e}\right)^2 - 5\left(\frac{u}{u_e}\right)^3 + 2\left(\frac{u}{u_e}\right)^4\right]. \tag{3.6}$$

The streamwise wall skin friction is assumed to be given by the well known two-dimensional relationship due to Ludwieg and Tillmann[5]

$$\frac{\tau_{01}}{\rho u_e^2} = 0{\cdot}123 \times 10^{-0{\cdot}678H} \left(\frac{u_e \theta_{11}}{\nu}\right)^{-0{\cdot}268} \tag{3.7}$$

or by a relationship due to Young[6]

$$\frac{\tau_{01}}{\rho u_e^2} = 0{\cdot}0088 \left(\frac{u_e \theta_{11}}{\nu}\right)^{-1/5}. \tag{3.8}$$

The cross-flow skin-friction component τ_{02} is taken to be $\tau_{01} \tan \beta$ with

$$\tan \beta = \operatorname*{Lim}_{\zeta \to 0} v/u. \tag{3.8}$$

4. *Shape-Factor Prediction in Three Dimensions.*

In order to predict the shape factor in three dimensions it is desirable that we first consider the established two-dimensional methods. Cooke[7] in fact did this in the case of small cross flow with an application of Spence's[8] method. This yielded fair results in one case and very poor results in another. Thompson[9] however has shown that most two-dimensional methods, including Spence's method, can be unreliable when used in situations very different from those from which they were initially derived. Thompson, however, shows that Head's[1] method is generally more reliable than other methods.

Head showed that if we assume the entrainment by the boundary layer of fluid from the external stream (i.e. the rate of change of volume flow in the boundary layer) to be a function of the velocity-profile shape, the external flow and some measure of the boundary-layer thickness an equation of the form

$$\frac{1}{u}\frac{d}{dx}\left[u(\delta - \delta^*)\right] = F(H_{\delta - \delta^*}) \tag{4.1}$$

is obtained. Here δ^* is the displacement thickness, δ the boundary layer thickness, u the velocity of the external stream, $H_{\delta-\delta^*} = (\delta - \delta^*)/\theta$ and θ is the boundary-layer momentum thickness. $F(H_{\delta-\delta^*})$ is a function derived by Head which he obtained by plotting $(1/u)\,(d/dx)\,[u(\delta - \delta^*)]$ against $H_{\delta-\delta^*}$ for several sets of experimental results.

As has been mentioned previously the streamwise velocity profiles in three-dimensional flow are similar to those in two-dimensional boundary layers. This being so we might hope to derive a similar equation to 4.1 for the three-dimensional case with due allowance being made for the convergence or divergence of the external streamlines and the effect of mass addition or subtraction through the sides of the control volume.

To do this we consider the continuity equation 2.4

$$\frac{1}{h_1 h_2}\frac{\partial (h_2 u)}{\partial \xi} + \frac{1}{h_1 h_2}\frac{\partial}{\partial \eta}(h_1 v) + \frac{\hat{c}_w}{\partial \zeta} = 0.$$

Integrating this term by term across the boundary layer yields

$$\frac{1}{h_2}\int_o^\delta \frac{1}{h_1}\frac{\partial (h_2 u)}{\partial \xi}\,d\zeta + \frac{1}{h_1}\int_o^\delta \frac{\partial}{h_2\,\partial \eta}(h_1 v)\,d\zeta + \int_o^\delta \frac{\partial w}{\partial \zeta}\,d\zeta = 0$$

$$\text{i.e.} \quad \frac{1}{h_2 h_1}\frac{\partial \int_0^{\delta} h_2 u d\zeta}{\partial \xi} - \frac{u_e}{h_1}\frac{\partial \delta}{\partial \xi} + \frac{1}{h_1 h_2}\frac{\partial \int_0^{\delta} h_1 v}{\partial \eta} d\zeta = -w_e \tag{4.2}$$

Writing

$$h_2 = r, \frac{1}{u_e} = h_1, \frac{1}{h_1}\frac{\partial}{\partial \xi} = \frac{\partial}{\partial s}, \frac{1}{h_2}\frac{\partial}{\partial \eta} = \frac{\partial}{\partial n} \text{ and } \delta_2 = -\int_o^{\delta} \frac{v}{u_e} d\zeta$$

4.2 becomes

$$\frac{1}{r}\frac{\partial (r \int_o^{\delta} u d\zeta)}{\partial s} - \frac{u_e \partial \delta_2}{\partial n} = \frac{u_e \partial \delta}{\partial s} - w_e, \tag{4.3}$$

where w_e signifies the value of w at the edge of the boundary layer. The terms on the right-hand side of 4.3 represent the entrainment of the external flow by the boundary layer and, following Head, we assume this to be a function of the streamwise velocity-profile shape, the external flow and some measure of the boundary-layer thickness. We choose these parameters to be $H_{\delta-\delta 1}$, u_e and $\delta - \delta_1$ respectively and rewrite 4.3 as

$$\frac{1}{r}\frac{\partial \left[r \int_0^{\delta} u d\zeta \right]}{\partial s} - u_e \frac{\partial \delta_2}{\partial n} = f(H_{\delta-\delta 1}, u_e, \delta - \delta_1)$$

or

$$\frac{1}{r}\frac{\partial [r u_e (\delta - \delta_1)]}{\partial s} - u_e \frac{\partial \delta_2}{\partial n} = f(H_{\delta-\delta 1}, u_e, \delta - \delta_1). \tag{4.4}$$

The left-hand side of equation 4.4 has the dimensions of a velocity so that 4.4 may be written as

$$\frac{1}{r}\frac{\partial [r u_e (\delta - \delta_1)]}{\partial s} - u_e \frac{\partial \delta_2}{\partial n} = u_e F(H_{\delta-\delta 1})$$

$$\frac{1}{u_e r}\frac{\partial [r u_e (\delta - \delta_1)]}{\partial s} - \frac{\partial \delta_2}{\partial n} = F(H_{\delta-\delta 1}). \tag{4.5}$$

Now Lighthill[10] has shown that the true displacement thickness δ^* is given by

$$\delta^* = \delta_1 + \frac{1}{u_e r}\frac{\partial}{\partial \eta}\int_o^{\xi} \delta_2 d\xi$$

Therefore

$$ru_e\delta^* = ru_e\delta_1 + \frac{\partial \int_o^\xi \delta_2 d\xi}{\partial \eta}.$$

$$\frac{\partial(ru_e\delta^*)}{\partial s} = \frac{\partial(ru_e\,\delta_1)}{\partial s} + \frac{1}{h_1}\frac{\partial \delta_2}{\partial \eta}$$

or

$$\frac{1}{u_e r}\frac{\partial(ru_e\delta^*)}{\partial s} = \frac{1}{u_e r}\frac{\partial(ru_e\delta_1)}{\partial s} + \frac{\partial \delta_2}{\partial n}. \tag{4.6}$$

Therefore 4.5 may be rewritten

$$\frac{1}{u_e r}\frac{\partial[ru_e(\delta-\delta^*)]}{\partial s} = F(H_{\delta-\delta 1}).$$

4.5 may also be written

$$\frac{1}{u_e}\frac{\partial[u_e(\delta-\delta_1)]}{\partial s} + (\delta-\delta_1)\frac{1}{r}\frac{\partial r}{\partial s} - \frac{\partial \delta_2}{\partial n} = F(H_{\delta-\delta 1})$$

and it will be seen that the second and third terms represent the effects due to convergence or divergence of the external streamlines and the addition or subtraction of mass through the sides of the control volume respectively.

5. *Approximate Solutions of the Momentum-Integral Equations.*

Cooke[7] made the assumption of small cross flow velocity and hence the momentum-integral equations took the form

$$\frac{\partial \theta_{11}}{\partial s} + \theta_{11}\left[(H+2)\frac{1}{u_e}\frac{\partial u_e}{\partial s} + \frac{1}{r}\frac{\partial r}{\partial s}\right] = \frac{\tau_{01}}{\rho u_e{}^2} \tag{5.1}$$

$$\frac{\partial \theta_{21}}{\partial s} + 2\theta_{21}\left[\frac{1}{u_e}\frac{\partial u_e}{\partial s} + \frac{1}{r}\frac{\partial r}{\partial s}\right] + \frac{1}{u_e r}\frac{\partial u_e}{\partial \eta}(\theta_{11}+\delta_1) = \frac{\tau_{02}}{\rho u_e{}^2} \tag{5.2}$$

He then assumed that H is constant and equal to 1·5 and that $\tau_{01}/\rho u_e{}^2 = 0{\cdot}0088\,(u_e\,\theta_{11}/v)^{-1/5}$. This resulted in 5.1 becoming

$$\frac{\partial(\Theta u_e{}^4 r^{1\cdot 2})}{\partial s} = 0{\cdot}0106\,u_e{}^4 r^{1\cdot 2} \tag{5.3}$$

where

$$\Theta = \theta_{11}\left(\frac{u_e\,\theta_{11}}{v}\right)^{1/5}.$$

For the solution of equation 5.2 he assumed that the streamwise and cross-flow velocity profiles are given by 3.2 and 3.3 respectively, i.e.

$$\frac{u}{u_e} = \left(\frac{\zeta}{\delta}\right)^{\frac{H-1}{2}}, \frac{v}{u_e} = \left(1-\frac{\zeta}{\delta}\right)^2 \frac{u}{u_e}\alpha$$

where $\alpha = \tan\beta \doteq \beta$ and β is the angle between the limiting and external streamlines. Then once more assuming that H is constant and equal to 1.5 he obtained 5.2 in the form

$$\frac{\partial\bar{\varepsilon}}{\partial s} + \frac{0{\cdot}0166\bar{\varepsilon}}{\Theta} = \frac{2{\cdot}187}{u_e^{2{\cdot}5}} \frac{\partial u_e}{\partial\eta} \tag{5.4}$$

where

$$\bar{\varepsilon} = \beta r u_e^{-3/2}.$$

This method has been programmed in Mercury Autocode for solution on the University of London Atlas Computer.

As will be mentioned in greater detail in Section 7, results with this method did not agree well with experiment and so the cross flow term $(1/r)\,(\partial\theta_{12}/\partial\eta)$ was next included in the streamwise momentum-integral equation. We now work with the equations

$$\frac{\partial\theta_{11}}{\partial s} + \frac{1}{r}\frac{\partial(\theta_{12})}{\partial\eta} + \theta_{11}\left[(H+2)\frac{1}{u_e}\frac{\partial u_e}{\partial s} + \frac{1}{r}\frac{\partial r}{\partial s}\right] = \frac{\tau_{01}}{\rho u_e^2} \tag{5.5}$$

and

$$\frac{\partial\theta_{21}}{\partial s} + 2\theta_{21}\left[\frac{1}{u_e}\frac{\partial u_e}{\partial s} + \frac{1}{r}\frac{\partial r}{\partial s}\right] + \frac{1}{u_e r}\frac{\partial u_e}{\partial\eta}(\theta_{11}+\delta_1) = \frac{\tau_{02}}{\rho u_e^2}. \tag{5.2}$$

Assuming the velocity profiles 3.2 and 3.3 we find

$$\theta_{12} = \alpha\delta\left[-\frac{1}{H} + \frac{4}{H+1} - \frac{1}{H+2} - \frac{4}{H+3} + \frac{2}{H+5}\right] \tag{5.6}$$

and

$$\theta_{11} = \frac{\delta(H-1)}{H(H+1)} \qquad \theta_{21} = \frac{-2\alpha\delta}{H(H+1)(H+2)}.$$

In the general case the derivative with respect to η would have to be first ignored, whilst a solution for several streamlines was obtained, and then accounted for by iteration. In the case of the infinite yawed wing to be considered here, however, we find that we may write

$$\frac{1}{r}\frac{\partial}{\partial\eta} = -\frac{v_1}{u_1}\frac{\partial}{\partial s}$$

where u_1, v_1 are velocity components in the x,y axes respectively, x and y are cartesian co-ordinates normal and parallel to the leading edge of the wing respectively. Thus, consider axes s and n along and

normal to the external streamline respectively inclined at angle ϕ to the x,y axes so that $\tan\phi = v_1/u_1$ and $u_e^2 = u_1^2 + v_1^2$. Then

$$x = s\cos\phi - n\sin\phi$$

$$y = s\sin\phi + n\cos\phi$$

$$\frac{\partial}{\partial s} = \frac{\partial}{\partial x}\frac{\partial x}{\partial s} + \frac{\partial}{\partial y}\frac{\partial y}{\partial s} = \frac{u_1}{u_e}\frac{\partial}{\partial x}$$

$$\frac{\partial}{\partial n} = \frac{\partial}{\partial x}\frac{\partial x}{\partial n} + \frac{\partial}{\partial y}\frac{\partial y}{\partial n} = -\frac{v_1}{u_e}\frac{\partial}{\partial x}.$$

(The derivatives with respect to y vanish as the wing is infinite and yawed).

$$\text{Hence } \frac{1}{r}\frac{\partial}{\partial \eta} = \frac{\partial}{\partial n} = -\frac{v_1}{u_1}\frac{\partial}{\partial s}.$$

We now assume that H is constant and equal to 1.5. It will be shown in greater detail in Section 7 that the variation of H only produces small changes to the results obtained from the streamwise momentum-integral equation but it may have significant effects upon the prediction of β the angle between the limiting and external streamlines particularly if β is large and $\partial H/\partial s$ significant. However, with the assumption of constant H we find that 5.6 becomes $\theta_{21} = -8/7\ \alpha\theta_{11}$, $\theta_{12} = 0{\cdot}498\alpha\theta_{11}$. The momentum-integral equations 5.5 and 5.2 may therefore be rewritten as

$$\frac{\partial\theta_{11}}{\partial s} - 0{\cdot}498\alpha\frac{v_1}{u_1}\frac{\partial\theta_{11}}{\partial s} - 0{\cdot}498\theta_{11}\frac{v_1}{u_1}\frac{\partial\alpha}{\partial s} = \frac{\tau_{01}}{\rho u_e^2} - \theta_{11}\left[(H+2)\frac{1}{u_e}\frac{\partial u_e}{\partial s} + \frac{1}{r}\frac{\partial r}{\partial s}\right]$$

$$-\frac{8}{7}\alpha\frac{\partial\theta_{11}}{\partial s} - \frac{8}{7}\theta_{11}\frac{\partial\alpha}{\partial s} = \alpha\frac{\tau_{01}}{\rho u_e^2} + \frac{16}{7}\alpha\theta_{11}\left[\frac{1}{u_e}\frac{\partial u_e}{\partial s} + \frac{1}{r}\frac{\partial r}{\partial s}\right]$$

$$+\frac{v_1}{u_1}\frac{1}{u_e}\frac{\partial u_e}{\partial s}\theta_{11} \quad (2{\cdot}5).$$

We now assume that $\tau_{01}/\rho u_e^2 = 0{\cdot}0088(u_e\theta_{11}/\nu)^{-1/5}$ and thus have two simultaneous differential equations in the two unknowns, θ_{11} and α. These have been recast into a form in which they could be solved on the computer by means of a step-by-step process involving a library routine of the Runge-Kutta-Merson type.

These equations are

$$\frac{\partial\theta_{11}}{\partial s} = \phi_1 - 0{\cdot}436\frac{v_1}{u_1}\phi_2$$

$$\frac{\partial\alpha}{\partial s} = -0{\cdot}875\frac{\phi_2}{\theta_{11}} - \frac{\alpha}{\theta_{11}}\frac{\partial\theta_{11}}{\partial s}$$

where

$$\phi_1 = 0{\cdot}0088\left(\frac{u_e\theta_{11}}{\nu}\right)^{-1/5} - \theta_{11}\left[\frac{3{\cdot}5}{u_e}\frac{\partial u_e}{\partial s} + \frac{1}{r}\frac{\partial r}{\partial s}\right]$$

$$\phi_2 = 0{\cdot}0088\alpha\left(\frac{u_e\theta_{11}}{\nu}\right)^{-1/5} + \frac{16}{7}\alpha\theta_{11}\left[\frac{1}{u_e}\frac{\partial u_e}{\partial s} + \frac{1}{r}\frac{\partial r}{\partial s}\right] + \frac{v_1}{u_1}\frac{2{\cdot}5}{u_e}\theta_{11}\frac{\partial u_e}{\partial s}$$

A comparison of the results obtained by the use of this method, known as Method 1, and those obtained experimentally will be made in Section 7.

After the extension of Head's[1] entrainment hypothesis to the three-dimensional case had been derived, an attempt was then made to include the variation of H in the streamwise momentum-integral equation for small cross flow 5.1 and simultaneously to calculate H. This will be known as Method 2.

The entrainment equation is

$$\frac{1}{u_e r}\frac{\partial[ru_e(\delta-\delta_1)]}{\partial s} - \frac{\partial\delta_2}{\partial n} = F(H_{\delta-\delta 1}).$$

If small cross flow is assumed we have

$$\frac{1}{u_e r}\frac{\partial[ru_e(\delta-\delta_1)]}{\partial s} = F(H_{\delta-\delta 1}). \tag{5.7}$$

We assume $F(H_{\delta-\delta 1})$ and $H_{\delta-\delta 1}$ as a function of H to be given by Head's curves and use the analytic form for these curves quoted by Standen[16],

$$\left.\begin{aligned} H_{\delta-\delta 1} &= 1{\cdot}535\,(H-0{\cdot}7)^{-2{\cdot}715} + 3{\cdot}3 \\ F(H_{\delta-\delta 1}) &= 0{\cdot}0306\,(H_{\delta-\delta 1}-3{\cdot}0)^{-{\cdot}653}. \end{aligned}\right\} \tag{5.8}$$

We now assume that $\tau_{o1}/\rho u_e{}^2$ is given by the Ludwieg-Tillmann[5] relation

$$\frac{\tau_{01}}{\rho u_e{}^2} = 0{\cdot}123\times 10^{-0{\cdot}678H}\left(\frac{u_e\theta_{11}}{\nu}\right)^{-0{\cdot}268}$$

and thus have two simultaneous differential equations for θ_{11} and $\delta-\delta_1$ i.e.

$$\frac{\partial\theta_{11}}{\partial s} + \theta_{11}\left[(H+2)\frac{1}{u_e}\frac{\partial u_e}{\partial s} + \frac{1}{r}\frac{\partial r}{\partial s}\right] = 0{\cdot}123\times 10^{-0{\cdot}678H}\left(\frac{u_e\theta_{11}}{\nu}\right)^{-0{\cdot}268} \tag{5.9}$$

$$\frac{\partial(\delta-\delta_1)}{\partial s} = 0{\cdot}0306\left[\frac{(\delta-\delta_1)}{\theta_{11}} - 3{\cdot}0\right]^{-{\cdot}653} - (\delta-\delta_1)\left[\frac{1}{r}\frac{\partial r}{\partial s} + \frac{1}{u_e}\frac{\partial u_e}{\partial s}\right] \tag{5.10}$$

and

$$H = \left[\frac{\dfrac{\delta-\delta_1}{\theta_{11}} - 3{\cdot}3}{1{\cdot}535}\right]^{-1/2{\cdot}715} + 0{\cdot}7$$

from 5.8 above. This method has also been programmed for solution on the computer.

It is also possible to include the variation of H in the momentum integral equations 5.5 and 5.2 allowing

for cross-flow. We thus have the three equations

$$\frac{\partial(\delta-\delta_1)}{\partial s} = F(H_{\delta-\delta 1})-(\delta-\delta_1)\left[\frac{1}{r}\frac{\partial r}{\partial s}+\frac{1}{u_e}\frac{\partial u_e}{\partial s}\right]$$

$$\frac{\partial\theta_{11}}{\partial s}+\frac{\partial(\theta_{12})}{\partial n} = \frac{\tau_{01}}{\rho u_e{}^2}-\frac{1}{u_e}\frac{\partial u_e}{\partial s}\theta_{11}[H+2]-\theta_{11}\frac{1}{r}\frac{\partial r}{\partial s} = \phi_1$$

$$\frac{\partial\theta_{21}}{\partial s} = \frac{\tau_{02}}{\rho u_e{}^2}-2\theta_{21}\left(\frac{1}{u_e}\frac{\partial u_e}{\partial s}+\frac{1}{r}\frac{\partial r}{\partial s}\right)-\theta_{11}(H+1)\frac{1}{u_e}\frac{\partial u_e}{\partial n} = \phi_2 .$$

We now assume the velocity profiles 3.2 and 3.3 so that from 5.6 we have

$$\theta_{21} = f_1(H)\,\theta_{11}\,\alpha = -\frac{2\theta_{11}\,\alpha}{(H-1)(H+2)} \tag{5.11}$$

and

$$\theta_{12} = f_2(H)\,\theta_{11}\,\alpha = \frac{\theta_{11}\,\alpha\,H(H+1)}{(H-1)}\left[-\frac{1}{H}+\frac{4}{H+1}-\frac{1}{H+2}-\frac{4}{H+3}+\frac{2}{H+5}\right] .$$

We also assume that the skin-friction term is given by the Ludwieg-Tillmann relation and we have $\partial/\partial n = -(v_1/u_1)(\partial/\partial s)$. The momentum-integral equations may thus be written as

$$\frac{\partial\theta_{11}}{\partial s}+\frac{v_1}{u_1}f_2\frac{\partial(\theta_{11}\,\alpha)}{\partial s}-\frac{v_1}{u_1}\theta_{11}\,\alpha\frac{\partial f_2}{\partial s} = \phi_1 \tag{5.12}$$

$$\theta_{11}\,\alpha\frac{\partial f_1}{\partial s}+f_1\frac{\partial\theta_{11}\,\alpha}{\partial s} = \phi_2 \tag{5.13}$$

Hence substituting for $\partial(\theta_{11}\,\alpha)/\partial s$ in 5.12 from 5.13 we obtain

$$\frac{\partial\theta_{11}}{\partial s}+\frac{v_1}{u_1}\alpha\,\theta_{11}\left[\frac{f_2}{f_1}\frac{\partial f_1}{\partial s}-\frac{\partial f_2}{\partial s}\right] = \phi_1+\frac{v_1}{u_1}\frac{f_2}{f_1}\phi_2 = \alpha_1$$

or

$$\frac{\partial\theta_{11}}{\partial s}+\frac{v_1}{u_1}\alpha\,\theta_{11}\frac{\partial H}{\partial s}\left[\frac{f_2}{f_1}\frac{\partial f_1}{\partial H}-\frac{\partial f_2}{\partial H}\right] = \alpha_1$$

or

$$\frac{\partial\theta_{11}}{\partial s}+\frac{v_1}{u_1}\alpha\,\alpha_2\frac{dH}{dH_{\delta-\delta 1}}\left[\frac{\partial(\delta-\delta_1)}{\partial s}-H_{\delta-\delta 1}\frac{\partial\theta_{11}}{\partial s}\right] = \alpha_1$$

where

$$\alpha_2 = \frac{f_2}{f_1}\frac{\partial f_1}{\partial H}-\frac{\partial f_2}{\partial H}$$

so that

$$\frac{\partial\theta_{11}}{\partial s} = \left[\alpha_1 - \frac{v_1}{u_1}\alpha\alpha_2\frac{dH}{dH_{\delta-\delta 1}}\frac{\partial(\delta-\delta_1)}{\partial s}\right] \Big/ \left[1-\frac{v_1}{u_1}\alpha\alpha_2 H_{\delta-\delta 1}\frac{dH}{dH_{\delta-\delta 1}}\right] . \tag{5.14}$$

5.13 may be rewritten as

$$\frac{\partial\alpha}{\partial s} = \left[\phi_2 - \alpha\theta_{11}\frac{\partial f_1}{\partial s} - f_1\alpha\frac{\partial\theta_{11}}{\partial s}\right] \Big/ f_1\theta_{11}$$

or

$$\frac{\partial\alpha}{\partial s} = \left[\phi_2 - f_1\alpha\frac{\partial\theta_{11}}{\partial s} - \alpha\frac{\partial f_1}{\partial H}\frac{dH}{\partial H_{\delta-\delta 1}}\left(\frac{\partial(\delta-\delta_1)}{\partial s} - H_{\delta-\delta 1}\frac{\partial\theta_{11}}{\partial s}\right)\right] \Big/ f_1\theta_{11} \tag{5.15}$$

and we have also that

$$\frac{\partial(\delta-\delta_1)}{\partial s} = 0{\cdot}0306\,(H_{\delta-\delta 1}-3{\cdot}0)^{-{\cdot}653} - (\delta-\delta_1)\left[\frac{1}{r}\frac{\partial r}{\partial s} + \frac{1}{u_e}\frac{\partial u_e}{\partial s}\right] . \tag{5.16}$$

From 5.8 we have

$$H_{\delta-\delta 1} = 1{\cdot}535\,(H-0{\cdot}7)^{-2{\cdot}715} + 3{\cdot}3$$

so that

$$H = \left[\frac{H_{\delta-\delta 1}-3{\cdot}3}{1{\cdot}535}\right]^{1/2{\cdot}715} + 0{\cdot}7$$

and

$$\frac{dH}{dH_{\delta-\delta_1}} = -\frac{\left[\dfrac{H_{\delta-\delta_1}-3{\cdot}3}{1{\cdot}535}\right]^{-1{\cdot}368}}{4{\cdot}1675}$$

In this form the equations have once more been programmed for solution on the Atlas computer.

It is also possible to include the cross-flow term, $\partial(\delta_2)/\partial n$ in the entrainment equation. This has been done here and will be known as Method 4. We have the equations

$$\frac{\partial(\delta-\delta_1)}{\partial s} - \frac{\partial\delta_2}{\partial\eta} = (\delta-\delta_1)\left[-\frac{1}{r}\frac{\partial r}{\partial s} - \frac{1}{u_e}\frac{\partial u_e}{\partial s}\right] + F\,(H_{\delta-\delta 1}) = \phi_3 \tag{5.17}$$

$$\frac{\partial\theta_{11}}{\partial s} + \frac{\partial\theta_{12}}{\partial n} = \frac{\tau_{01}}{\rho u_e{}^2} - \frac{1}{u_e}\frac{\partial u_e}{\partial s}\theta_{11}\,(H+2) - \theta_{11}\frac{1}{r}\frac{\partial r}{\partial s} = \phi_1$$

$$\frac{\partial\theta_{21}}{\partial s} = \frac{\tau_{02}}{\rho u_e{}^2} - 2\theta_{21}\left(\frac{1}{u_e}\frac{\partial u_e}{\partial s} + \frac{1}{r}\frac{\partial r}{\partial s}\right) - \theta_{11}\,(H+1)\frac{1}{u_e}\frac{\partial u_e}{\partial n} = \phi_2 .$$

We now make the same assumptions for the velocity profiles and skin friction as we did in Method 3, so that

$$\frac{\tau_{01}}{\rho u_e^2} = \cdot 123 \times 10^{-0\cdot 678H} \left(\frac{u_e \theta_{11}}{\nu}\right)^{-\cdot 268}$$

$$\theta_{21} = f_1 \theta_{11} \alpha = -\frac{2\theta_{11}\alpha}{(H-1)(H+2)}$$

$$\frac{\partial \theta_{11}}{\partial s} = \frac{\alpha_1}{\alpha_4} + \frac{\alpha_4 - 1}{\alpha_4} \frac{\partial(\delta - \delta_1)}{\partial s} \tag{5.14}$$

and

$$\frac{\partial \alpha}{\partial s} = \left[\phi_2 - \alpha\theta_{11}\frac{\partial f_1}{\partial s} - f_1 \alpha \frac{\partial \theta_{11}}{\partial s}\right] \Big/ f_1 \theta_{11} \tag{5.15}$$

and in this form the equations 5.19, 5.14 and 5.15 have been programmed for solution on the computer.

In addition to his expression for the cross-flow velocity profile 3.4 Eichelbrenner[3] has suggested a calculation method which is not restricted to the case of small cross flow. For the shape parameter equation he multiplies the streamwise equation of motion by u and then integrates with respect to ζ to obtain the three-dimensional counterpart of the energy integral equation. The term which appears on the right-hand side of this equation

$$\int_o^\delta \tau_1 \frac{\partial u}{\partial \zeta} d\zeta$$

he assumed to be given by a two-dimensional expression due to Rotta:

$$\frac{\int_o^\delta \tau_1 \frac{\partial u}{\partial \zeta} d\zeta}{\rho u_e^3} = 0{\cdot}0056 \left(\frac{u_e \theta_{11}}{\nu}\right)^{-1/6}.$$

This type of technique does not yield as good results as the entrainment approach in two dimensions[11] and so a method has been developed which uses the entrainment approach together with the quartic (3.6) velocity profile. This will be known as Method 5.

The use of the quartic velocity profile

$$\frac{v}{u_e} = \alpha \left[\frac{u}{u_e} - 3\left(\frac{u}{u_e}\right)^2 + 3\left(\frac{u}{u_e}\right)^3 - \left(\frac{u}{u_e}\right)^4\right] - c \left[3\left(\frac{u}{u_e}\right)^2 - 5\left(\frac{u}{u_e}\right)^3 + 2\left(\frac{u}{u_e}\right)^4\right]$$

together with the form for the streamwise profile

$$\frac{u}{u_e} = \left(\frac{\zeta}{\delta}\right)^n$$

yields

$$\theta_{12} = f_2 \theta_{11} \alpha = \theta_{11} \alpha \frac{H(H+1)}{H-1} \left[-\frac{1}{H} + \frac{4}{H+1} - \frac{1}{H+2} - \frac{4}{H+3} + \frac{2}{H+5}\right]$$

and in addition

$$\delta_2 = \int_o^\delta \frac{v}{u_e} d\zeta = -\frac{16\,\alpha\,\theta_{11}\,H}{(H-1)\,(H+3)\,(H+5)} = -f_3\,\alpha\,\theta_{11}\,. \tag{5.18}$$

5.17 may therefore be written as

$$\frac{\partial(\delta-\delta_1)}{\partial s} - \frac{v_1}{u_1} f_3 \frac{\partial \theta_{11}\alpha}{\partial s} - \frac{v_1}{u_1}\alpha\theta_{11}\frac{\partial f_3}{\partial s} = \phi_3\,.$$

Substituting for $\partial(\alpha\theta_{11})/\partial s$ from 5.13 gives

$$\frac{\partial(\delta-\delta_1)}{\partial s} + \frac{v_1}{u_1}\alpha\theta_{11}\left[\frac{f_3}{f_1}\frac{\partial f_1}{\partial s} - \frac{\partial f_3}{\partial s}\right] = \phi_3 + \frac{v_1}{u_1}\frac{f_3}{f_1}\phi_2$$

or

$$\frac{\partial(\delta-\delta_1)}{\partial s} + \frac{v_1}{u_1}\alpha\theta_{11}\frac{\partial H}{\partial s}\left[\frac{f_3}{f_1}\frac{\partial f_1}{\partial H} - \frac{\partial f_3}{\partial H}\right] = \phi_3 + \frac{v_1}{u_1}\frac{f_3}{f_1}\phi_2$$

$$\frac{\partial(\delta-\delta_1)}{\partial s} + \frac{v_1}{u_1}\alpha\left[\frac{f_3}{f_1}\frac{\partial f_1}{\partial H} - \frac{\partial f_3}{\partial H}\right]\frac{dH}{dH_{\delta-\delta 1}}\left[\frac{\partial(\delta-\delta_1)}{\partial s} - H_{\delta-\delta 1}\frac{\partial \theta_{11}}{\partial s}\right] = \phi_3 + \frac{v_1}{u_1}\frac{f_3}{f_1}\phi_2\,.$$

But from 5.14

$$\frac{\partial \theta_{11}}{\partial s} = \frac{\alpha_1}{\alpha_4} + \frac{\alpha_4 - 1}{\alpha_4}\frac{\partial(\delta-\delta_1)}{\partial s}$$

where

$$\alpha_1 = \phi_1 + \frac{v_1}{u_1}\frac{f_2}{f_1}\phi_2\,,\ \alpha_4 = 1 - \frac{v_1}{u_1}\alpha\,\alpha_2\,H_{\delta-\delta 1}\frac{dH}{dH_{\delta-\delta 1}}$$

so that we may write

$$\frac{\partial(\delta-\delta_1)}{\partial s}(1+\alpha_5) - \alpha_5\,H_{\delta-\delta 1}\left[\frac{\alpha_1}{\alpha_4} + \left(\frac{\alpha_4-1}{\alpha_4}\right)\frac{\partial(\delta-\delta_1)}{\partial s}\right] = \phi_3 + \frac{v_1}{u_1}\frac{f_3}{f_1}\phi_2$$

or

$$\frac{\partial(\delta-\delta_1)}{\partial s}\left[1+\alpha_5 - \alpha_5\,H_{\delta-\delta 1}\left(\frac{\alpha_4-1}{\alpha_4}\right)\right] = \phi_3 + \alpha_5\,H_{\delta-\delta 1}\frac{\alpha_1}{\alpha_4} + \frac{v_1}{u_1}\frac{f_3}{f_1}\phi_2 \tag{5.19}$$

where

$$\alpha_5 = \frac{v_1}{u_1}\alpha\left[\frac{f_3}{f_1}\frac{\partial f_1}{\partial H} - \frac{\partial f_3}{\partial H}\right]\frac{\partial H}{\partial H_{\delta-\delta 1}}$$

From Method 3 we also have

$$\theta_{11} = \int_o^\delta \left(1-\frac{u}{u_e}\right)\frac{u}{u_e}\,d\zeta = \frac{\delta n}{(n+1)(2n+1)}, \delta_1 = \int_o^\delta 1-\frac{u}{u_e}\,d\zeta = \frac{\delta n}{n+1}$$

so that

$$H = \frac{\delta_1}{\theta_{11}} = 2n+1$$

and

$$\delta_2 = -\int_o^\delta \frac{v}{u_e}\,d\zeta = -\delta\left[\alpha\left(\frac{1}{n+1}-\frac{3}{2n+1}+\frac{3}{3n+1}-\frac{1}{4n+1}\right) - c\left(\frac{3}{2n+1}-\frac{5}{3n+1}+\frac{2}{4n+1}\right)\right]$$

$$\theta_{21} = -\int_o^\delta \frac{uv}{u_e^2}\,d\zeta = -\delta\left[\alpha\left(\frac{1}{2n+1}-\frac{3}{3n+1}+\frac{3}{4n+1}-\frac{1}{5n+1}\right) - c\left(\frac{3}{3n+1}-\frac{5}{4n+1}+\frac{2}{5n+1}\right)\right]$$

$$\theta_{12} = \int_0^\delta \frac{v}{u_e}-\frac{uv}{u_e^2}\,d\zeta = -\delta_2+\theta_{21} = -\delta\left[\alpha\left(\frac{1}{n+1}-\frac{4}{2n+1}+\frac{6}{3n+1}-\frac{4}{4n+1}+\frac{1}{5n+1}\right)\right.$$
$$\left. - c\left(\frac{3}{2n+1}-\frac{8}{3n+1}+\frac{7}{4n+1}-\frac{2}{5n+1}\right)\right] \qquad (5.20)$$

$$\theta_{22} = -\int_o^\delta \frac{v^2}{u_e^2}\,d\zeta = -\delta\left[\alpha^2\left(\frac{1}{2n+1}-\frac{6}{3n+1}+\frac{15}{4n+1}-\frac{20}{5n+1}+\frac{15}{6n+1}-\frac{6}{7n+1}+\frac{1}{8n+1}\right)\right.$$
$$-2\alpha c\left(\frac{3}{3n+1}-\frac{14}{4n+1}+\frac{26}{5n+1}-\frac{24}{6n+1}+\frac{11}{7n+1}-\frac{2}{8n+1}\right)$$
$$\left.+c^2\left(\frac{9}{4n+1}-\frac{30}{5n+1}+\frac{37}{6n+1}-\frac{20}{7n+1}-\frac{4}{8n+1}\right)\right]$$

With these assumptions we may reduce all the quantities in the momentum and entrainment equations to functions of θ_{11}, α, c and H. At this stage however we have only three equations and four unknowns so a further equation is required.

Eichelbrenner[3] has suggested an equation which relates c to the external flow, which for irrotational flow may be written

$$\frac{\partial c}{\partial s} = -c\left(\frac{1}{r}\frac{\partial r}{\partial s}-\frac{1}{u_e}\frac{\partial u_e}{\partial s}\right)-\frac{2}{u_e}\frac{\partial u_e}{\partial n} \qquad (5.21)$$

This equation has been accepted here. As before in the general case derivatives with respect to n would have to be accounted for by iteration but in the case of the infinite yawed wing we may write $\partial/\partial n =$

$-(v_1/u_1)(\partial/\partial s)$ and so include them directly. This being done we have four equations in the four unknowns, θ_{11}, c, α and H, which after rearrangement have been programmed for solution on the computer. These equations are not given here because, as will be mentioned in greater detail in Section 7, this method yielded unrealistic values for the angle between the limiting and external streamlines.

The main features of all the methods outlined above are listed for easy reference in Table 1.

All the momentum-integral equations mentioned above include the term $(1/r)(\partial r/\partial s)$. Cooke[7] has shown that for an infinite yawed wing

$$r = A\frac{u_1}{u_e}$$

where u_1 is the velocity component of the free stream normal to the leading edge of the wing and A is an arbitrary constant. We may therefore write

$$\frac{1}{r}\frac{\partial r}{\partial s} = \frac{u_e}{u_1}\frac{\partial}{\partial s}(u_1/u_e) \tag{5.22}$$

but

$$u_e^2 = u_1^2 + v_1^2$$

and v_1 is a constant. We have also that

$$\frac{\partial}{\partial s} = \frac{u_1}{u_e}\frac{\partial}{\partial x}$$

so that 5.22 becomes

$$\frac{1}{r}\frac{\partial r}{\partial s} = \frac{u_e}{u_1}\frac{\partial}{\partial s}(u_1/u_e) = \frac{v_1^2}{u_e^3}\frac{du_1}{dx} = \frac{v_1^2}{u_1 u_e^2}\frac{\partial u_1}{\partial s} = \frac{v_1^2}{u_1^2}\frac{1}{u_e}\frac{\partial u_e}{\partial s} \tag{5.23}$$

by means of which the term $(1/r)(\partial r/\partial s)$ has been accounted for in all the computations mentioned above.

6. *The Experimental Measurements.*

The model used to obtain three-dimensional turbulent boundary layers was basically a flat plate swept at $26\frac{1}{2}$ deg and mounted horizontally between vertical false walls in the 30 in × 39 in working section of the Queen Mary College low-speed blowdown wind tunnel. Beneath this plate and also swept at $26\frac{1}{2}$ deg was a porous circular cylinder fitted with a Thwaites[12] flap. Boundary-layer suction was applied to the cylinder to prevent boundary-layer separation. The Thwaites flap could be put at any desired angle and the distance between the cylinder and plate varied so that different pressure distributions could be obtained on the plate. This somewhat unusual arrangement was used in preference to a simple swept wing as it offered the advantage of a flat surface on which to measure the boundary layer so that traverses normal to the surface were easily accomplished.

By using a constant-temperature hot-wire anemometer the boundary-layer velocity profiles in both magnitude and direction were measured along the centreline of the plate for the nine pressure distributions shown in Figure 1. The theoretical prediction of these pressure distributions was accomplished by means of an extension of a theory which had been developed for an unswept version of the apparatus.

Further details of the apparatus and measurement techniques will be omitted as it is hoped to publish these in full detail together with details of all the measured velocity profiles as a separate report.

7. *Comparison of Theory with Experiment.*

7.1. *The Prediction of Momentum Thickness.*

All the velocity profiles mentioned in Section 6 have been analysed to obtain experimental values of θ_{11} the streamwise momentum thickness, β the angle of the limiting streamline and H the streamwise shape factor. Cooke's theory and the five other theories detailed in Section 5 have then been used to predict theoretically the variation of these parameters for each of the nine runs. The results for streamwise momentum thickness are shown plotted against x, the distance normal to the leading edge of the plate, in Figures 2 to 10. In each case the theory was started at $x = 4{\cdot}34$ in and again at $x = 15{\cdot}97$ in, the first point measured in the adverse pressure gradient. The start at $x = 4{\cdot}34$ in rather than at 2·55 in was chosen as the pressure distribution was not given accurately by the theory at the latter value.

For easy reference the main features of the methods under test are listed in Table I.

There are two series of Runs, Runs 1 to 5 and Runs 6 to 9, the pressure gradients are highest in Run 1 and lowest in Run 5 for the first series, and highest in Run 6 and lowest in Run 9 for the second series (*see* Figure 1).

Dealing first with the prediction of streamwise momentum thickness θ_{11} as shown in Figures 2 and 10 it is immediately apparent that apart from Run 1 (Figure 2) there is a discrepancy between the experimental points and the theoretical predictions. Moreover the magnitude of this discrepancy appears to increase as the values of the pressure gradients involved decrease. This being so, it seems hardly likely that the discrepancies are due to cross-flow effects, which might be expected to be greatest at the higher pressure gradients, especially as will be shown below, the theories seem to take reasonable account of these. Nor does it seem likely that the discrepancies can be attributed to departure of the experimental conditions from those pertaining to an infinite yawed wing, as here also it might reasonably be supposed that these departures would be greatest in the cases involving the larger pressure gradients. It appears possible, therefore that the skin-friction term $\tau_{01}/\rho u_e^2$ is responsible as this will assume greater importance in the momentum-integral equation as the magnitude of the pressure gradient decreases. To account for the observed discrepancies in Figures 2 to 10 the skin friction term $\tau_{01}/\rho u_e^2$ would have to be lower in the case of a diverging flow with a favourable pressure gradient and higher in the case of a converging flow with an adverse pressure gradient than would be so in the two-dimensional case.

In an effort to be more precise about this an attempt was made to evaluate the magnitude of the skin-friction term for the Runs 1, 2 and 5, used in Table 2, by accounting for all the other terms in the momentum integral equations. Unfortunately to do this the term $d\theta_{11}/\partial s$ must be obtained from graphical differentiation of the experimental results. This latter procedure is always difficult and in this case there are too few points for $\partial\theta_{11}/\partial s$ to be evaluated to a degree of accuracy which would ensure a meaningful figure for the resulting value of the skin-friction term $\tau_{01}/\rho u_e^2$. To resolve this matter the direct measurement of the skin friction would have had to be attempted which, in the circumstances, was out of question.

Another possible if less likely explanation for the discrepancy between experiment and theory is that certain terms which have been neglected in the derivation of the equations may not necessarily be negligible in this case. These terms are such that if they are included the streamwise boundary-layer equation becomes

$$\frac{u\partial u}{h_1\partial\xi}+\frac{v}{h_2}\frac{\partial u}{\partial\eta}+\frac{w\,\partial u}{\partial\zeta}-k_2\,uv+k_1\,v^2 =$$

$$-\frac{1}{\rho h_1}\frac{\partial p}{\partial\xi}+\frac{1}{\rho}\frac{\partial}{\partial\zeta}\left[\mu\frac{\partial u}{\partial\zeta}-\rho\overline{(u'w')}\right]-\frac{1}{h_2}\frac{\partial(\overline{u'v'})}{\partial\eta}-\frac{1}{h_1}\frac{\partial(\bar{u}'^2)}{\partial\xi}.$$

The terms in question are the last two on the right-hand side. Of these the term $\dfrac{1}{h_1}\dfrac{\partial(\bar{u}'^2)}{\partial\xi}$ is generally neglected on the assumption that rates of change in the ξ direction are far smaller than those in the ζ direction.

The other term $-\frac{1}{h_2}\frac{\partial(\overline{u'v'})}{\partial\eta}$ would be zero in a two-dimensional boundary layer and we might hope to neglect it here on the grounds that rates of change in the η direction are far smaller than those in the ζ direction. Turcotte[13] suggested that this term might be responsible for the discrepancy between experiment and theory found by Ashkenas and Riddell[14] for the growth of a turbulent boundary layer on a yawed flat plate. Ashkenas[15] made an attempt to measure this term but states that his measurements were of questionable validity although they did indicate that $-\frac{1}{h_2}\frac{\partial(\overline{u'v'})}{\partial\eta}$ was of the correct sign but too small a magnitude to explain the discrepancy found by Ashkenas and Riddell. The effect of this term in the present series of experiments is a matter which could only be settled by further experiment and unfortunately the author is no longer in a position to do this.

As mentioned above an analysis of the orders of magnitude of the various terms in the streamwise momentum-integral equation has been made in the case of three runs, numbers 1, 2 and 5, and is presented in Table 2. We rewrite the momentum-integral equation in the form

$$\frac{\partial\theta_{11}}{\partial s}=\frac{\tau_{01}}{\rho u_e^2}-\frac{\partial(\theta_{12})}{\partial n}-\frac{1}{u_e}\frac{\partial u_e}{\partial s}(2\theta_{11}+\delta_1)-\frac{1}{r}\frac{\partial r}{\partial s}(\theta_{11})+\frac{1}{r}\frac{\partial r}{\partial s}(\theta_{22}) \tag{7.1, 1}$$

The terms $(1/u_e)/(\partial u_e/\partial s)$ and $(1/r)/(\partial r/\partial s)$ have been calculated from the theoretical pressure distribution and θ_{11}, δ_1 and θ_{22} are taken from the experimental measurements. The term $\partial(\theta_{12})/\partial n$ has been obtained by graphical differentiation of the measured values of θ_{12}. The skin-friction term is as given by the Ludwieg-Tillmann[5] relation but as mentioned above this may well be in error. It is immediately apparent from study of Table 2 that the last term on the right-hand side, $(1/r)\,(\partial r/\partial s)\,(\theta_{22})$, is negligible in comparison with the other terms. The term $\partial(\theta_{12})/\partial n$ would appear to be at least of the same magnitude as the term $\theta_{11}(1/r)\,(\partial r/\partial s)$. This cross flow term $\partial(\theta_{12})/\partial n$ would appear generally to amount to less than 10 per cent of the total $\partial\theta_{11}/\partial s$ and study of Figures 3 to 10 reveals that the increments in θ_{11} predicted by those theories (2, 3, 4 and 5) which attempt to account for this term are greater by this amount than those which do not. The comparison here should be made between Cooke's method, which does not allow for the cross-flow term, and Method 1 which does, and between Method 2, which allows H to vary but does not allow for this term, and Methods 3 and 4, which also have H varying and account for the cross-flow term. This would appear to confirm that the cross flow is adequately accounted for by the present theories. Figures 2 to 10 also indicate that the variation of H has little effect upon the final result as is the case in two dimensions for moderate pressure gradients.* An increase in H increases the magnitude of the term $(1/u_e)\,(\partial u_e/\partial s)\,(2\theta_{11}+\delta_1)$ but decreases the magnitude of the term $\tau_{o1}/\rho u_e^2$, the net result being little or no change in the value of $\partial\theta_{11}/\partial s$. It will also be noticed that Methods 3 and 4 coincide as might be expected from the above-mentioned insensitivity of the streamwise momentum-integral equation to H, the only difference between Methods 3 and 4 being the inclusion of a small cross-flow term in the shape-parameter equation. To summarize it would appear that the cross-flow terms in the streamwise momentum-integral equation are fairly small for chordwise pressure gradients of the order investigated, thus giving some support to Cooke's original assumption, although they may amount to 10 per cent of $\partial\theta_{11}/\partial s$, but the skin-friction term may be significantly different from that in the corresponding two-dimensional case and some experimental determination of the magnitude of the terms neglected in the derivation of the streamwise momentum equation is desirable.

*This may be seen by comparing the results obtained by the use of Cooke's method, which assumes small cross flow and H constant, with the results obtained by Method 2 which also assumes small cross flow but includes the variation of H.

7.2. *The Prediction of* β.

Turning to the prediction of β, the angle between the limiting and external streamlines, shown in Figures 11 to 19, it will be seen that the agreement between experiment and theory is in general quite good apart from the predictions of Cooke's method and Method 1 in the region 10 in $< x <$ 16 in for all runs and for $x > 10$ in for run 6. It will be recalled that Cooke's method and Method 1 are the only methods, of those tested, which do not include the variation of H, the streamwise shape parameter. Rewriting the cross-wise momentum-integral equation 2.10 in the form

$$\frac{\partial \theta_{21}}{\partial s} = \frac{\tau_{02}}{\rho u_e^2} - 2\theta_{21}\left[\frac{1}{u_e}\frac{\partial u_e}{\partial s} + \frac{1}{r}\frac{\partial r}{\partial s}\right] - \frac{1}{u_e}\frac{\partial u_e}{\partial n}(\theta_{11} + \delta_1) \tag{7.2, 1}$$

it will be remembered that for Cooke's method and Methods 1 to 4, θ_{21} was obtained in terms of β, H and θ_{11} by means of the relation

$$\theta_{21} = \frac{2\beta\theta_{11}}{(H-1)(H+2)}$$

so that

$$\frac{\partial \theta_{21}}{\partial s} = -\frac{2}{(H-1)(H+2)}\left[\frac{\beta \partial \theta_{11}}{\partial s} + \theta_{11}\frac{\partial \beta}{\partial s}\right] + \beta\theta_{11}\frac{\partial H}{\partial s}\left[\frac{1}{(H-1)(H+2)}\right] \tag{7.2, 2}$$

substituting in 7.2.1 gives

$$\frac{\partial \beta}{\partial s} = -\frac{(H-1)(H+2)}{2\theta_{11}}\left[\beta\frac{\tau_{01}}{\rho u_e^2} - \frac{1}{u_e}\frac{\partial u_e}{\partial n}(\theta_{11} + \delta_1)\right]$$
$$-2\beta\left[\frac{1}{u_e}\frac{\partial u_e}{\partial s} + \frac{1}{r}\frac{\partial r}{\partial s}\right] + \beta\frac{\partial H}{\partial s}. \tag{7.2, 3}$$

For Cooke's method and Method 1, H is taken to be constantly equal to 1.5 so that the last term on the right-hand side of equation 7.2.3 is assumed to be zero. This will clearly not be so should β be large and $\partial H/\partial s$ be significant as is the case for Run 6 $x > 16$ in. In the other cases of failure mentioned above for $x > 10$ in we have β small and $(1/u_e)(\partial u_e/\partial n)$ negative so that the first term on the right-hand side is negative. H is generally about 1·2 in this region so that the assumption of $H = 1{\cdot}5$ produces values of $\partial\beta/\partial s$ which are more negative than actually is the case as can be seen from Figures 11 to 19.

Method 5 has not been plotted in Figures 11 to 19 as it gave values of β which varied wildly. An example of this is shown in Figure 20. The reason for this is thought to be as follows. Method 5 assumes θ_{21} to be given by

$$\theta_{21} = -\delta\left[\alpha\left(\frac{1}{2n+1} - \frac{3}{3n+1} + \frac{4}{4n+1} - \frac{1}{5n+1}\right) - c\left(\frac{3}{3n+1} - \frac{5}{4n+1} + \frac{2}{5n+1}\right)\right] \tag{7.2, 4}$$

where

$$\alpha = \tan\beta$$

$$n = \frac{H-1}{2} \tag{7.2, 4}$$

and α and c are of the same size with c usually slightly greater than α. Taking a typical value of H, 1·4, and substituting in 7.2.4, and 7.2.3 gives

$$n = 0{\cdot}2$$
$$\theta_{21} = -\delta[\alpha(\cdot 006) - c(\cdot 1)] \tag{7.2, 5}$$

so that θ_{21} depends to a very much greater extent upon the value of c than upon the value of β. Similarly $\partial\theta_{21}/\partial s$ will depend much more upon the value of $\partial c/\partial s$ than upon the value of $\partial\beta/\partial s$. Unfortunately it is this latter much smaller term which we are attempting to calculate by allowing approximately for all the other terms in the cross-flow momentum-integral equation. In other words we are attempting to calculate the small difference of two large numbers neither of which are known exactly. This sort of procedure usually results in the type of result shown in Figure 20. It must be mentioned here that despite the doubt concerning one of the boundary conditions employed in its derivation, the quintic velocity profile 3·4 due to Eichelbrenner[3] was incorporated in a calculation method similar to Method 5 and similar wild variations in β resulted. The predictions for θ_{11} by this method were virtually identical with those given by Method 5.

7.3. *The Prediction of the Streamwise Shape Parameters H.*

The predictions for H as given by the various methods are shown in Figures 21 to 25. It will be seen that there are only slight differences between the predictions of the various methods, the greatest differences occurring, as would be expected, in those cases involving the largest cross flows. The difference between Methods 3 and 4 is that the latter includes the term $\partial\delta_2/\partial n$ in the entrainment equation 4.5 and it can be seen that, apart from when the cross flow is large, there is little to choose between them, thus confirming that the assumption of small cross flow for the entrainment equation in Method 3 was valid. The comparison between the experimentally determined value of H and the theoretical predictions is encouraging particularly when it is remembered that Cooke's attempt to apply Spence's two-dimensional method to three dimensions resulted, in one case, in values of H twice as large as those determined experimentally. The scatter of the experimental points for Run 6, $x < 13$ in, is rather large but the velocity profiles at these positions were rather unusual.

7.4. *The Prediction of the Parameter c.*

Method 5 involved the calculation of the variation of the parameter c by means of equation 5.2,1 due to Eichelbrenner[3]. Figures 26 to 29 compare the results obtained by the use of this equation with those obtained experimentally. The experimental values were determined from polar plots (v/u_e against u/u_e) of the velocity profiles. c is defined as

$$c = \operatorname*{Lim}_{u/u_e \to 1} \frac{v}{u - u_e}$$

and the large scatter of the experimental results reflects the difficulties involved in determining this quantity. These difficulties are naturally greatest when there is little or no cross flow as inaccuracies in the measurement of the flow direction then become dominant. This explains the odd values of c obtained for Run 1, $x = 9{\cdot}7$ in and 11·5 in and Run 6, 11·5 in. Although the scatter of the experimental points makes assessment difficult it would appear that equation 5.21 gives fair results for c. This point will not be pursued further because, as mentioned above, the use of this equation in Method 5 resulted in unrealistic values of the parameter β, and the knowledge of β is far more important than that of c as the former parameter is required to give some indication of three-dimensional separation.

5. *Conclusions.*

It has been shown that a discrepancy exists between the values of streamwise momentum thickness predicted by the theories detailed in Section 3 and those found experimentally. This discrepancy is thought

to be due to the skin-friction term not being adequately accounted for by a 'two-dimensional' expression or possibly if less likely to the neglect of certain terms in the derivation of the streamwise momentum-integral equation. Certainly, in any future experiments on three-dimensional turbulent boundary layers, it would be of great value if the magnitude of skin friction and the neglected terms could be measured directly although this is not to suggest that such measurements will be easy to accomplish.

The inclusion of the cross-flow terms in the streamwise momentum-integral equation results in the examples given here in a small improvement in the prediction of the streamwise momentum thickness. In the general case, unlike the infinite yawed wing considered here, these terms can only be accounted for by an iterative process. Where the cross-flow terms are manifestly small, however, it is debatable whether the increase in accuracy obtained by their inclusion is justified by the additional complexity involved in the calculation. Should their inclusion be required, however, the methods presented here appear to take reasonable account of them.

As in the two-dimensional case the variation of the shape parameter H produces little changes in the values of the streamwise momentum thickness from those obtained by the assumption that H is a constant. This assumption has been shown, however, to produce inaccurate values of β, the angle between the limiting and external streamlines, for cases involving small values of β and low values of H. This could of course to some extent be rectified by choice of a smaller constant value of H, but more serious errors in the prediction of β are to be found in cases in which β becomes large and $\partial H/\partial s$ becomes significant. For safety it would appear advisable to include the variation H in the prediction of β. This variation may be calculated by the extension of Head's entrainment hypothesis to the three-dimensional case, presented here. The use of the type of calculation procedure suggested by Eichelbrenner[3] appears, in the cases tested here, to suffer from the defect that β may not be calculated with any reliability.

Acknowledgements.

The author wishes to express his grateful thanks to Professor A. D. Young for all his assistance during the course of the research which formed the basis for this paper. Thanks are also due to Mr. G. Rutherford for his painstaking construction of the experimental apparatus. Finally thanks to my wife for typing the manuscript and preparing the original figures.

LIST OF SYMBOLS

ξ, η, ζ	Orthogonal curvilinear co-ordinates with ζ measured normal to the surface
h_1, h_2	Metrics in the ξ, η, ζ co-ordinate system ($h_3 = 1$)
u, v, w	Velocities in the ξ, η, ζ directions respectively
k_1	$= -\frac{1}{h_1 h_2} \frac{\partial h_2}{\partial \xi}$ geodesic curvature of the curve ξ = constant
k_2	$= -\frac{1}{h_1 h_2} \frac{\partial h_1}{\partial \eta}$ geodesic curvature of the curve η = constant
s, n	Directions along and normal to an external streamline respectively
r	$= h_2$
$\theta_{22}, \delta_1, \delta_2$ $\theta_{11}, \theta_{21}, \theta_{12}$	Displacement and momentum thicknesses defined by equation 2.11
τ_{01}, τ_{02}	Skin-friction components in the ξ, η directions respectively
H	$= \delta_1/\theta_{11}$ the streamwise shape parameter
$H_{\delta-\delta 1}$	$= (\delta - \delta_1)/\theta_{11}$ shape parameter used in entrainment theory
ρ	The density of the fluid
μ	The viscosity of the fluid
ν	μ/ρ the kinematic viscosity of the fluid
P	The static pressure in the fluid
x, y, z	Cartesian co-ordinates
Θ	$= \theta_{11} \left(\frac{u_e \theta_{11}}{\nu}\right)^{1/5}$ parameter used in Cooke's method, Section 5
$\bar{\varepsilon}$	$= \beta r u_e^{-3/2}$ parameter used in Cooke's method, Section 5
δ	The boundary-layer thickness
δ^*	The true displacement thickness
β	The angle between limiting and external streamlines
α	$= \tan \beta$
c	$= \underset{u/u_e \to 1}{\text{limit}} \frac{v}{u - u_e}$
Suffix e	External to the boundary layer

REFERENCES

No.	*Author(s)*	*Title, etc.*
1	M. R. Head	Entrainment in the turbulent boundary layer. A.R.C. R. & M. 3152. September 1958.
2	J. C. Cooke	Three-dimensional turbulent boundary layers. A.R.C. C.P. 635. June 1961.
3	E. A. Eichelbrenner	La couche limite tridimensionnelle en regime turbulent d'un fluide compressible : Cas de la paroi athermane. *Agardograph* 97, Part 2, pp. 801–828. May 1965.
4	J. P. Johnston	The three-dimensional turbulent boundary layer. M.I.T. Gas Turbine Lab. Rep. No. 39. 1957.
5	H. Ludwieg and W. Tillmann	Untersuchungen über die Wandscubspannung in turbulenten Reibungsschichten. *Ing. Arciv.* Vol. 17, p. 288, 1949. A.R.C. 14 800.
6	A. D. Young	The calculation of the profile drag of aerofoils and bodies of revolution at supersonic speeds. Coll. of Aeronautics Rep. 73, A.R.C. 15 970. 1953.
7	J. C. Cooke	A calculation method for three-dimensional turbulent boundary layers. A.R.C. R. & M. 3199. October 1958.
8	D. A. Spence	The development of turbulent boundary layers. *J. Aeronaut. Sci.* Vol. 23, No. 1, pp. 3–15. 1956.
9	B. G. Thompson	A critical review of existing methods of calculating the turbulent boundary layer. A.R.C. R. & M. 344. August 1964.
10	M. J. Lighthill	On displacement thickness. *J. Fluid Mech.* 4, pp. 383–392. 1958.
11	D. B. Spalding	The kinetic-energy-deficit equation of the turbulent boundary layer. *Agardograph* 97, Part 1, pp. 199–244. May 1965.
12	B. Thwaites	The production of lift independently of incidence. The Thwaites flap. Part I and II. A.R.C. R.& M. 2611. November 1947.
13	D. L. Turcotte	On incompressible turbulent boundary layer theory applied to infinite yawed bodies. Cornell Univ. Graduate School of Aero. Eng. 1955.
14	H. Ashkenas and F. R. Riddell	Investigation of the Turbulent boundary layer on a yawed flat plate. NACA TN 3383. 1955.
15	H. Ashkenas	Turbulent shearing stress in the boundary layer of yawed flat plates. NACA TN 4140. 1958.
16	N. M. Standen	A concept of mass entrainment applied to compressible turbulent boundary layers in adverse pressure gradients. A.I.A.A. Paper No. 64–584. 1964.

TABLE 1

The Turbulent Boundary-Layer Methods.

Cooke's Method	Assumes the streamwise shape parameter H to be constant and equal to 1·5. Assumes small cross-flow velocity and the velocity profiles to be given by $u/u_e = (\zeta/\delta)^{H-1/2}$ and $v/u_e = (1-\zeta/\delta)^2\,(u/u_e)\,\alpha$ with $\alpha = \tan\beta = \tau_{02}/\tau_{01}$, with $\tau_{01}/\rho u_e{}^2 = 0{\cdot}0088\,(u_e\,\theta_{11}/\nu)^{-1/5}$
Method 1	Not restricted to small cross-flow velocity. All other assumptions as for Cooke's method.
Method 2	Assumes small cross flow but allows for the variation of H in the streamwise momentum-integral equation by means of the equation $(1/u_e r)\,(\partial[r\,u_e\,(\delta-\delta_1)]/\partial s) = F\,(H_{\delta-\delta 1})$ with $H_{\delta-\delta 1} = 1{\cdot}535\,(H-0{\cdot}7)^{-2{\cdot}715}+3{\cdot}3$ and $F\,(H_{\delta-\delta 1}) = 0{\cdot}0306\,(H_{\delta-\delta 1}-3{\cdot}0)^{-{\cdot}653}$. The streamwise skin friction being given by the Ludwieg-Tillmann relation $\tau_{01}/\rho u_e{}^2 = 0{\cdot}123\times 10^{-0{\cdot}678H}\,(u_e\theta_{11}/\nu)^{-0{\cdot}268}$.
Method 3	Not restricted to small cross flow. Velocity profile assumptions as Method 1 but H calculated as for Method 2.
Method 4	As for Method 3 except that H is calculated by the equation $(1/u_e r)\,(\partial[r u_e\,(\delta-\delta_1)]/\partial s)-\partial\delta_2/\partial n = F\,(H_{\delta-\delta 1})$.
Method 5	Includes all the terms in both streamwise and cross-wise momentum-integral equations. Assumes the Ludwieg-Tillmann relation for the skin friction and the velocity profiles to be given by $\frac{u}{u_e} = \left(\frac{\zeta}{\delta}\right)^n$ and $\frac{v}{u_e} = \alpha\left[\frac{u}{u_e}-3\left(\frac{u}{u_e}\right)^2+3\left(\frac{u}{u_e}\right)^3-\left(\frac{u}{u_e}\right)^4\right]-c\left[3\left(\frac{u}{u_e}\right)^2-5\left(\frac{u}{u_e}\right)^3+2\left(\frac{u}{u_e}\right)^4\right]$. Calculates the variation of H by the same equation as Method 4.

TABLE 2

Orders of Magnitude of Terms in Streamwise Momentum-integral Equation.

	$\frac{\partial\theta_{11}}{\partial s} =$	$\frac{\tau_{01}}{\rho u_e^2}$	$-\frac{\partial\theta_{12}}{\partial n}$	$-\frac{1}{u_e}\frac{\partial u_e}{\partial s}(2\theta_{11}+\delta_1)$	$-\frac{1}{r}\frac{\partial r}{\partial s}(\theta_{11})$	$+\frac{1}{r}\frac{\partial r}{\partial s}(\theta_{22})$
	$x =$ 4·34 in	$2{\cdot}21 \times 10^{-3}$	$-3{\cdot}15 \times 10^{-4}$	$-1{\cdot}68 \times 10^{-3}$	$-1{\cdot}11 \times 10^{-4}$	$-2{\cdot}38 \times 10^{-6}$
	$x =$ 6·13 in	2·29 × „	$-2{\cdot}19 \times$ „	$-2{\cdot}76 \times$ „	$-1{\cdot}72 \times$ „	$-1{\cdot}87 \times$ „
R	$x =$ 7·92 in	2·38 × „	$-1{\cdot}68 \times$ „	$-4{\cdot}36 \times$ „	$-2{\cdot}35 \times$ „	$-5{\cdot}99 \times 10^{-7}$
	$x =$ 9·70 in	2·50 × „	$-0{\cdot}86 \times$ „	$-5{\cdot}44 \times$ „	$-2{\cdot}37 \times$ „	$-1{\cdot}23 \times$ „
U	$x =$ 11·49 in	1·88 × „	$-0{\cdot}06 \times$ „	$-5{\cdot}0 \times$ „	$-1{\cdot}67 \times$ „	$-8{\cdot}6 \times 10^{-8}$
N	$x =$ 15·97 in	2·06 × „	2·74 × „	7·86 × „	2·53 × „	$9{\cdot}4 \times 10^{-7}$
	$x =$ 17·75 in	1·63 × „	8·57 × „	$1{\cdot}0 \times 10^{-2}$	4·58 × „	$6{\cdot}6 \times 10^{-6}$
1	$x =$ 19·54 in	1·34 × „	$1{\cdot}04 \times 10^{-3}$	$8{\cdot}35 \times 10^{-3}$	4·42 × „	$1{\cdot}18 \times 10^{-5}$
	$x =$ 21·33 in	1·20 × „	1·23 × „	6·38 × „	3·74 × „	1·54 × „
	$x =$ 4·34 in	$2{\cdot}23 \times 10^{-3}$	$-4{\cdot}8 \times 10^{-4}$	$-1{\cdot}27 \times 10^{-3}$	$-8{\cdot}85 \times 10^{-5}$	$-2{\cdot}62 \times 10^{-6}$
R	$x =$ 6·13 in	2·35 × „	$-2{\cdot}57 \times$ „	$-2{\cdot}13 \times$ „	$-1{\cdot}39 \times 10^{-4}$	$-2{\cdot}38 \times$ „
	$x =$ 7·92 in	2·48 × „	$-1{\cdot}79 \times$ „	$-3{\cdot}11 \times$ „	$-1{\cdot}82 \times$ „	$-1{\cdot}27 \times$ „
U	$x =$ 9·70 in	2·58 × „	$-7{\cdot}21 \times 10^{-5}$	$-3{\cdot}95 \times$ „	$-1{\cdot}91 \times$ „	$-9{\cdot}2 \times 10^{-7}$
	$x =$ 11·49 in	2·55 × „	$-1{\cdot}84 \times$ „	$-4{\cdot}5 \times$ „	$-1{\cdot}7 \times$ „	$-2{\cdot}21 \times$ „
N						
	$x =$ 15·97 in	2·17 × „	$3{\cdot}52 \times 10^{-4}$	5·01 × „	2·02 × „	8·0 × „
2	$x =$ 17·75 in	1·71 × „	6·49 × „	8·25 × „	4·15 × „	$5{\cdot}0 \times 10^{-6}$
	$x =$ 19·54 in	1·43 × „	7·27 × „	6·52 × „	3·76 × „	$1{\cdot}03 \times 10^{-5}$
	$x =$ 21·33 in	1·47 × „	6·64 × „	4·17 × „	2·82 × „	$8{\cdot}06 \times 10^{-6}$
	$x =$ 4·34 in	$2{\cdot}11 \times 10^{-3}$	$-3{\cdot}84 \times 10^{-4}$	$-4{\cdot}47 \times 10^{-7}$	$-3{\cdot}5 \times 10^{-8}$	$-1{\cdot}08 \times 10^{-9}$
R	$x =$ 6·13 in	2·23 × „	$-2{\cdot}27 \times$ „	$-4{\cdot}0 \times 10^{-4}$	$-3{\cdot}13 \times 10^{-5}$	$-7{\cdot}2 \times 10^{-7}$
	$x =$ 7·92 in	2·35 × „	$-2{\cdot}24 \times$ „	$-1{\cdot}52 \times 10^{-3}$	$-9{\cdot}85 \times$ „	$-1{\cdot}79 \times 10^{-6}$
U	$x =$ 9·70 in	2·55 × „	$-1{\cdot}59 \times$ „	$-2{\cdot}44 \times$ „	$-1{\cdot}7 \times 10^{-4}$	$-2{\cdot}08 \times$ „
	$x =$ 11·49 in	2·5 × „	$-5{\cdot}4 \times 10^{-5}$	$-3{\cdot}26 \times$ „	$-1{\cdot}94 \times$ „	$-1{\cdot}36 \times$ „
N						
	$x =$ 15·97 in	2·08 × „	$2{\cdot}4 \times 10^{-4}$	4·8 × „	3·0 × „	1·99 × „
3	$x =$ 17·75 in	1·87 × „	3·41 × „	3·9 × „	2·76 × „	2·48 × „
	$x =$ 19·54 in	1·76 × „	1·95 × „	1·62 × „	1·22 × „	1·8 × „
	$x =$ 21·33 in	1·77 × „	$8{\cdot}05 \times 10^{-5}$	$3{\cdot}87 \times 10^{-4}$	$3{\cdot}0 \times 10^{-5}$	$4{\cdot}0 \times 10^{-7}$

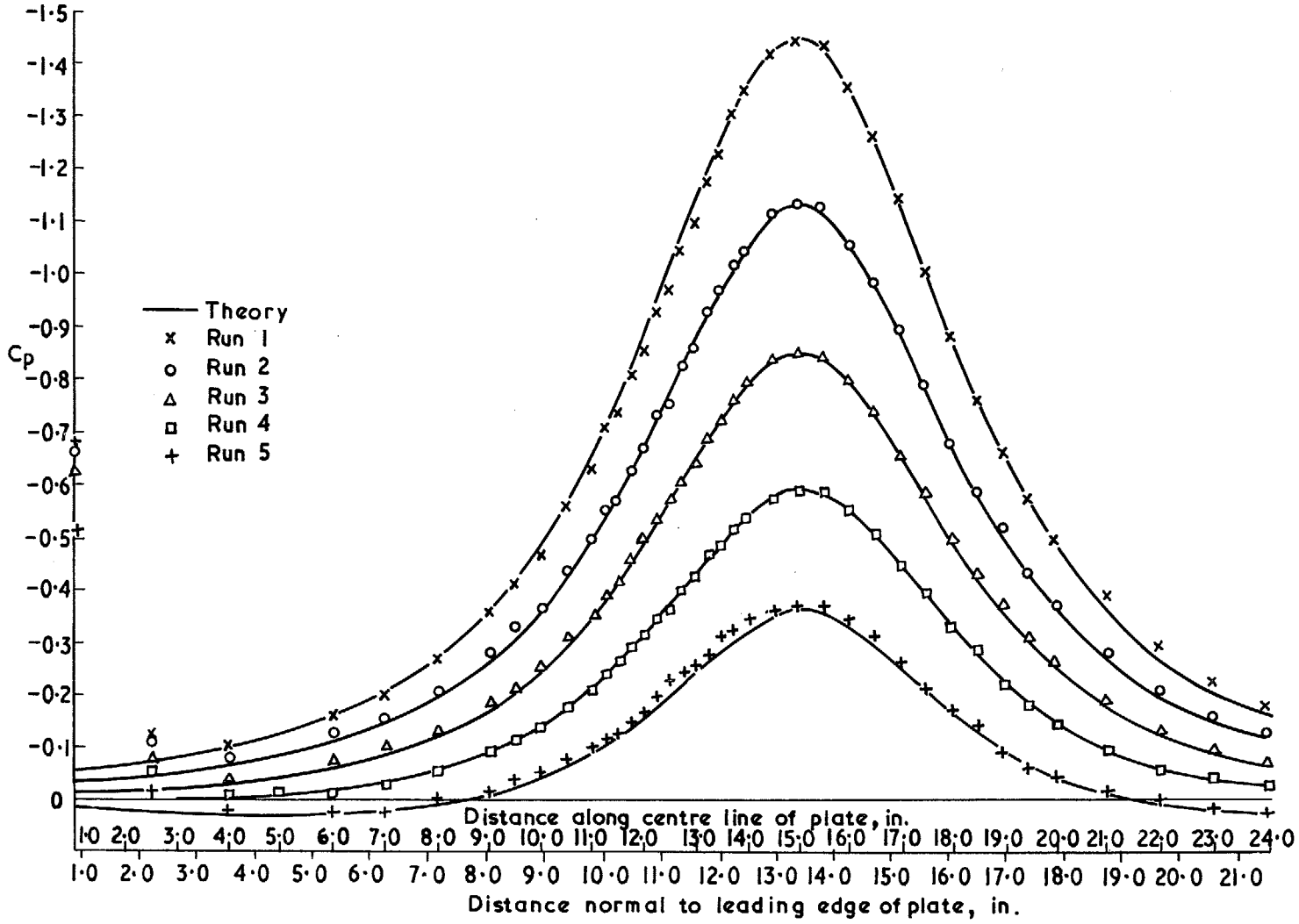

FIG. 1. Comparison of theoretical and experimental pressure distributions.

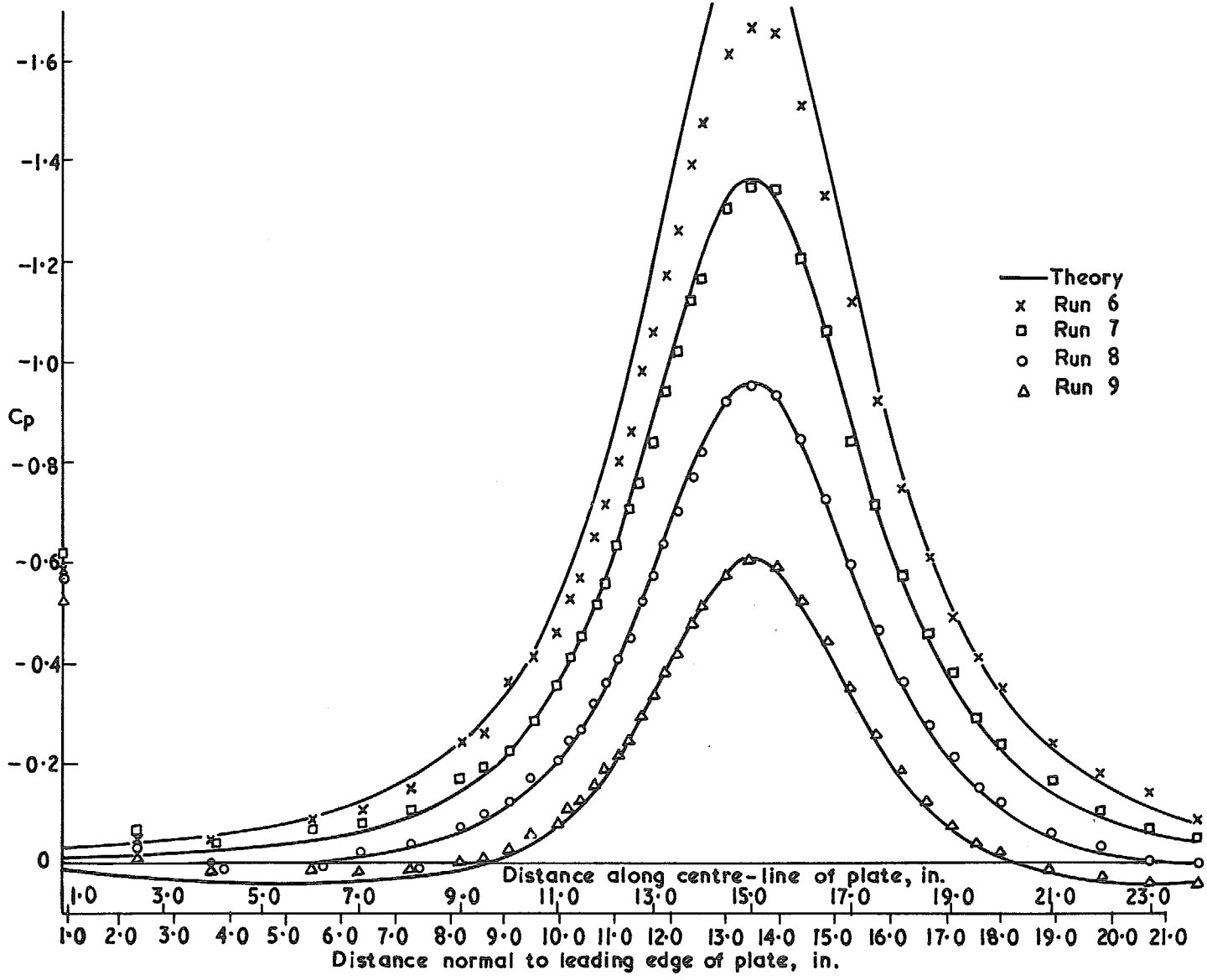

FIG. 1. (contd.). Comparison of theoretical and experimental pressure distributions.

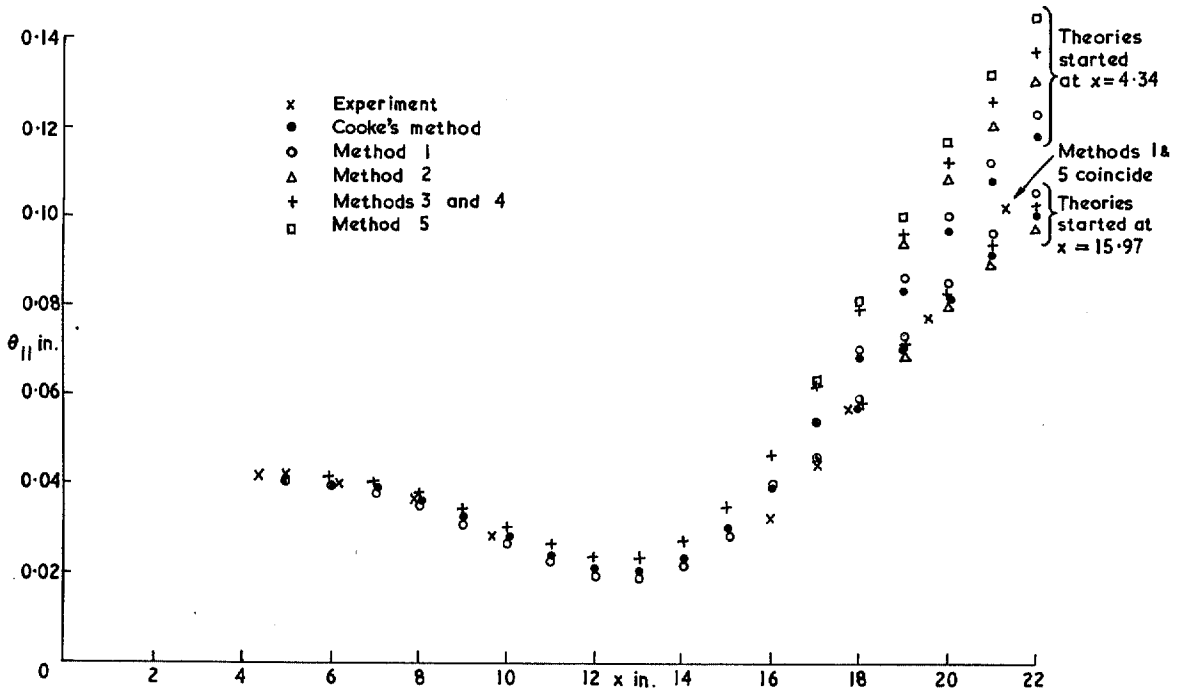

FIG. 2. Streamwise momentum thickness plotted against distance normal to the leading edge. Run 1.

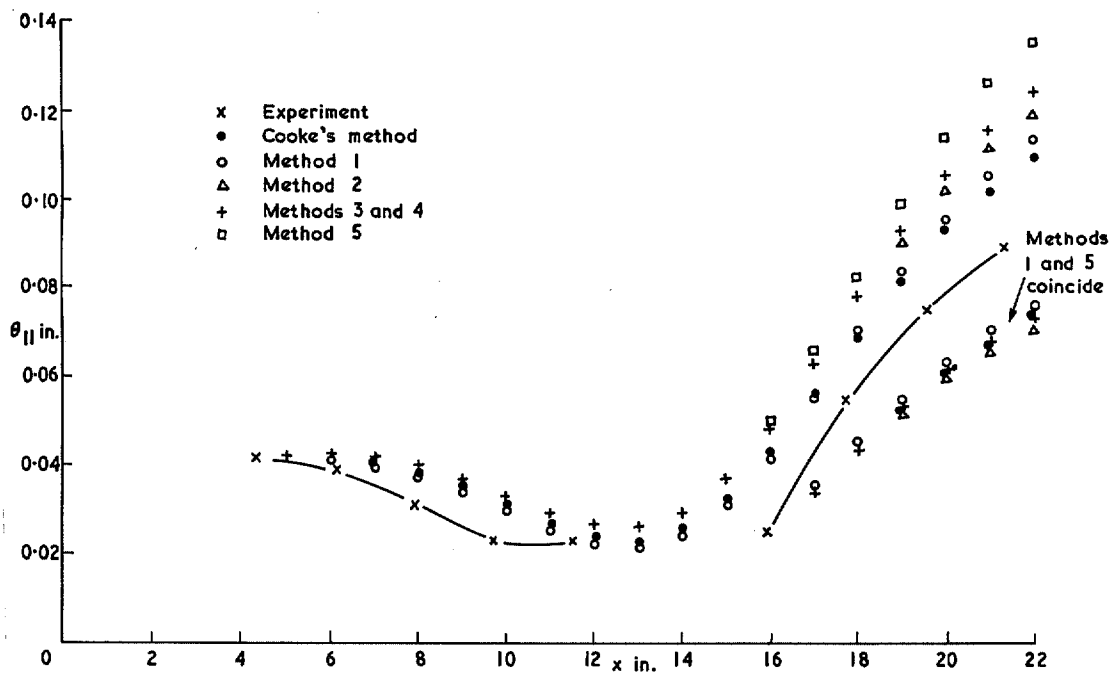

FIG. 3. Streamwise momentum thickness plotted against distance normal to the leading edge. Run 2.

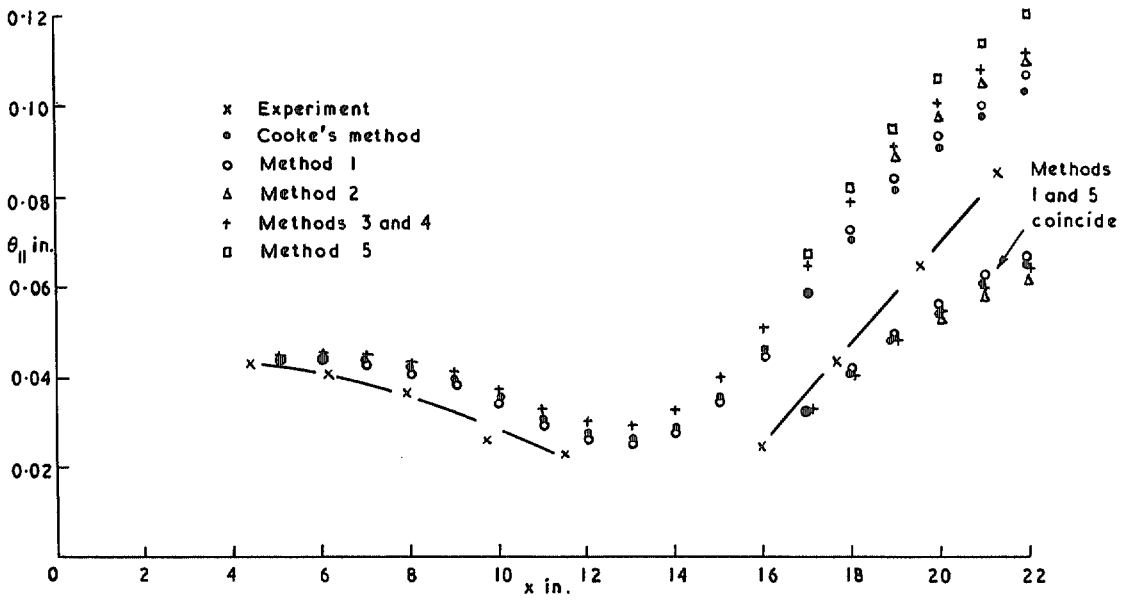

FIG. 4. Streamwise momentum thickness plotted against distance normal to the leading edge. Run 3.

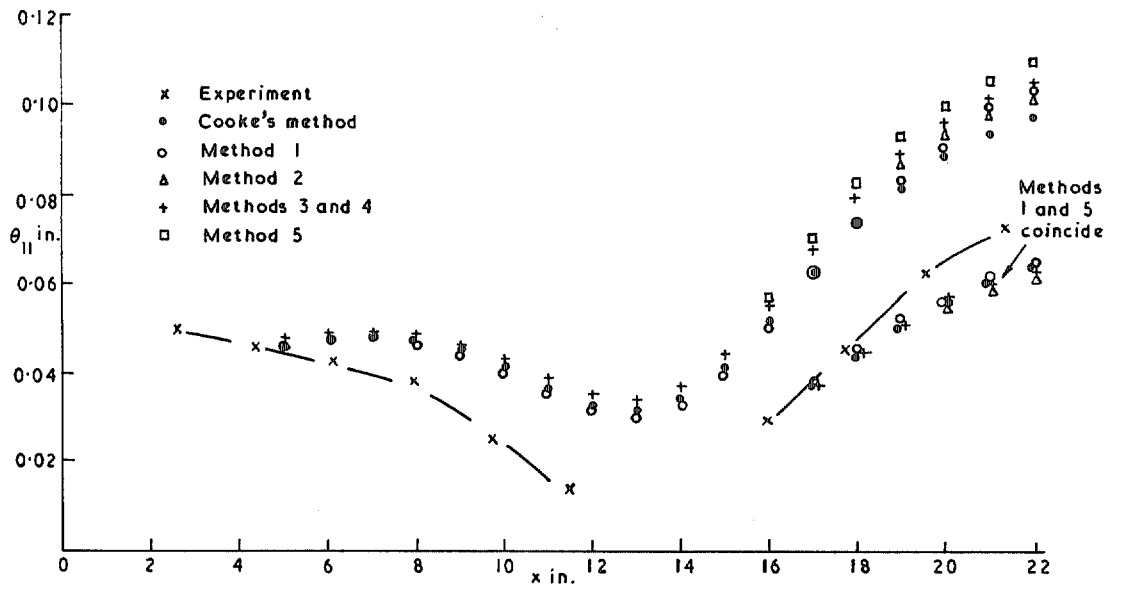

FIG. 5. Streamwise momentum thickness plotted against distance normal to the leading edge. Run 4.

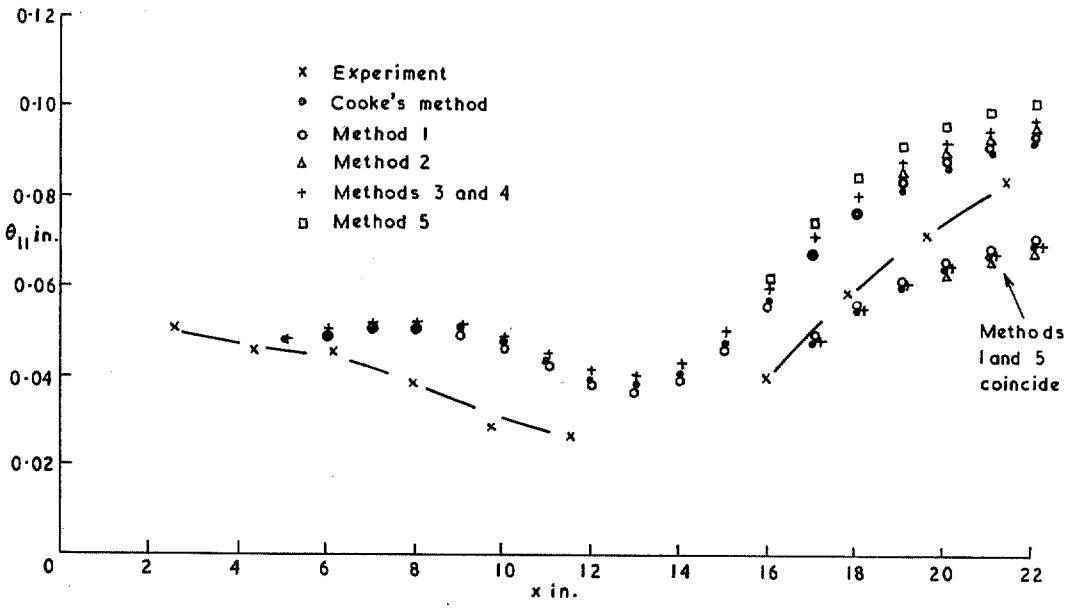

FIG. 6. Streamwise momentum thickness plotted against distance normal to the leading edge. Run 5.

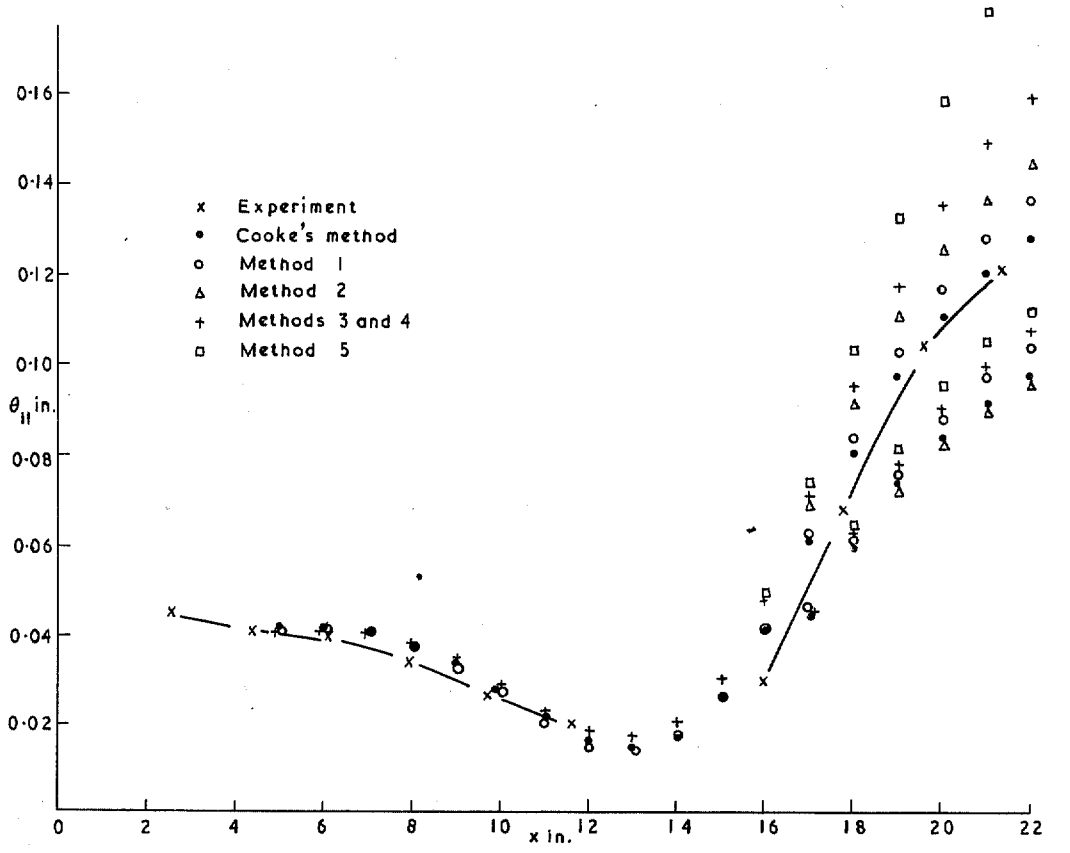

FIG. 7. Streamwise momentum thickness plotted against distance normal to the leading edge. Run 6.

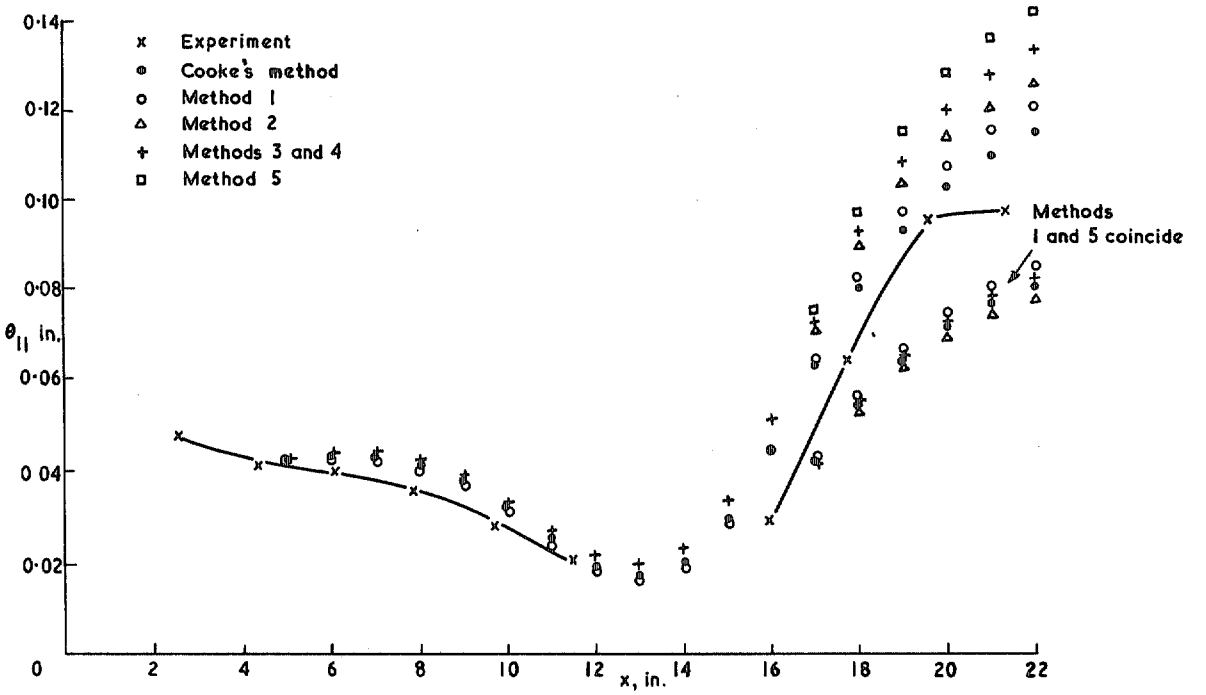

FIG. 8. Streamwise momentum thickness plotted against distance normal to the leading edge. Run 7.

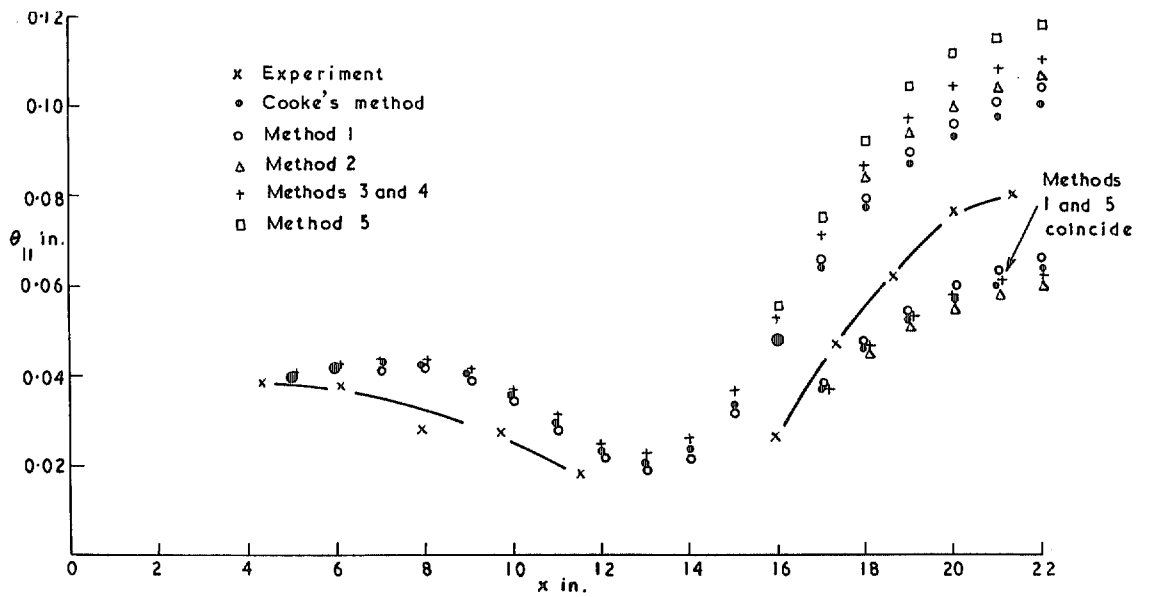

FIG. 9. Streamwise momentum thickness plotted against distance normal to the leading edge. Run 8.

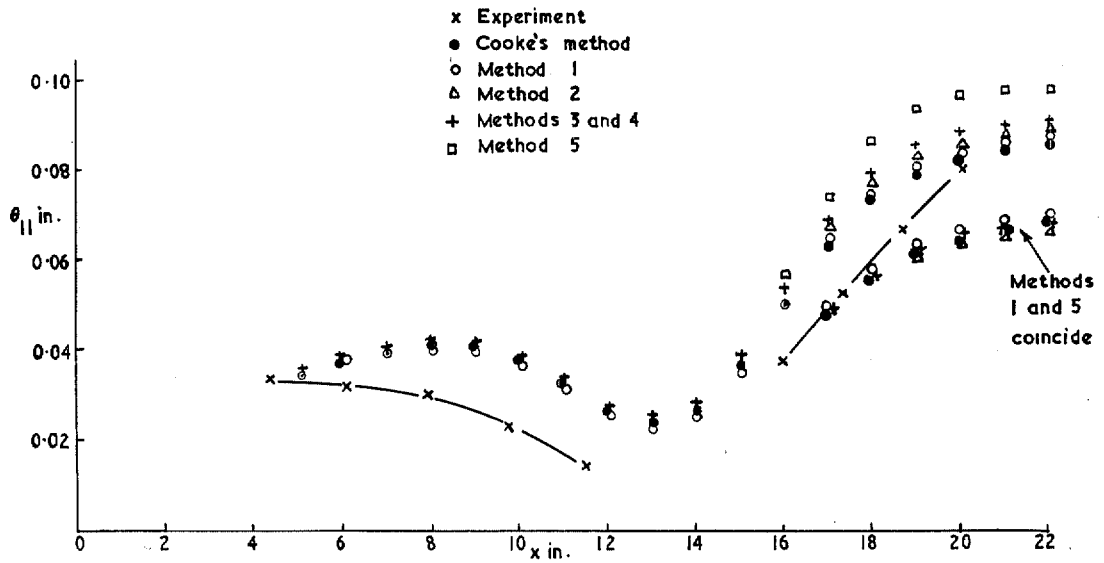

FIG. 10. Streamwise momentum thickness plotted against distance normal to the leading edge. Run 9.

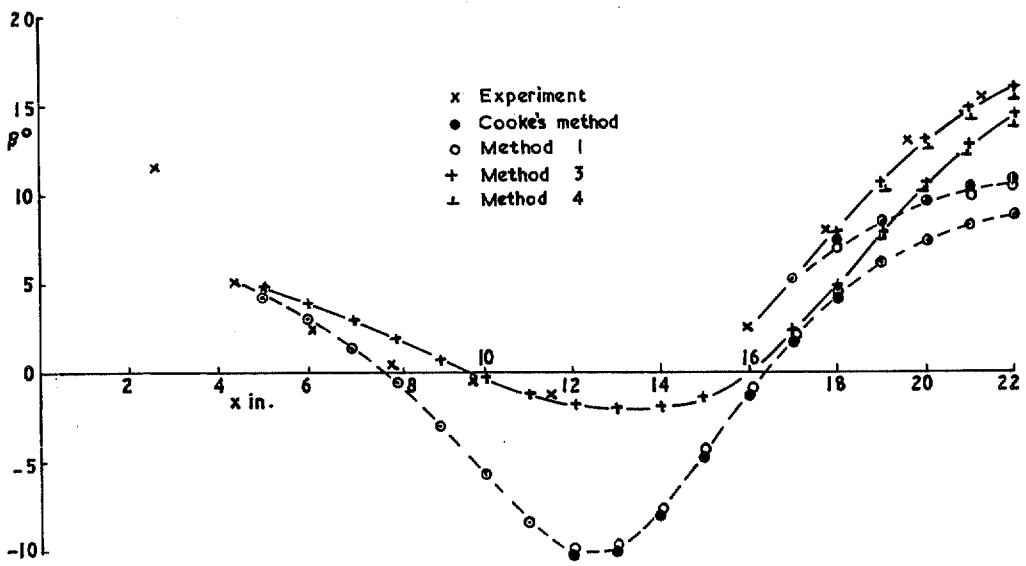

FIG. 11. Angle between limiting and external streamlines plotted against distance normal to the leading edge. Run 1.

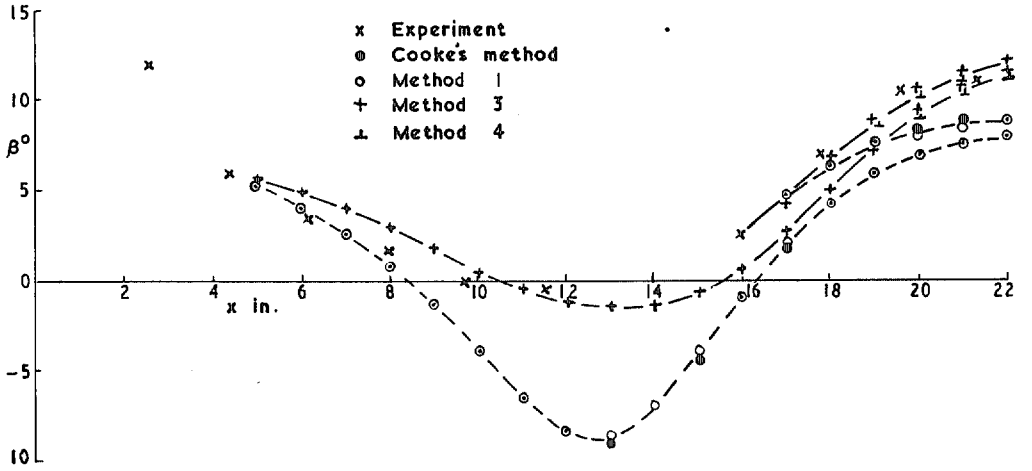

FIG. 12. Angle between limiting and external streamlines plotted against distance normal to the leading edge. Run 2.

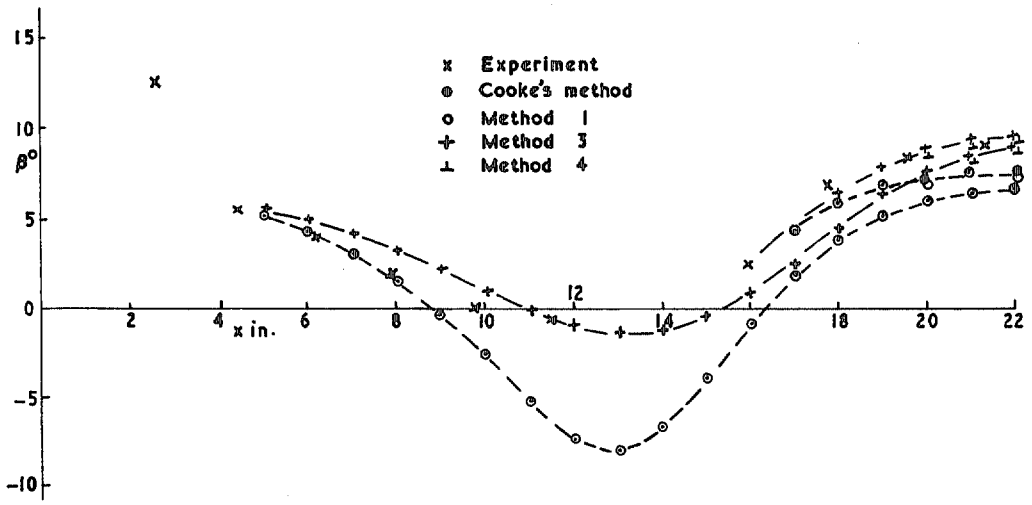

FIG. 13. Angle between limiting and external streamlines plotted against distance normal to the leading edge. Run 3.

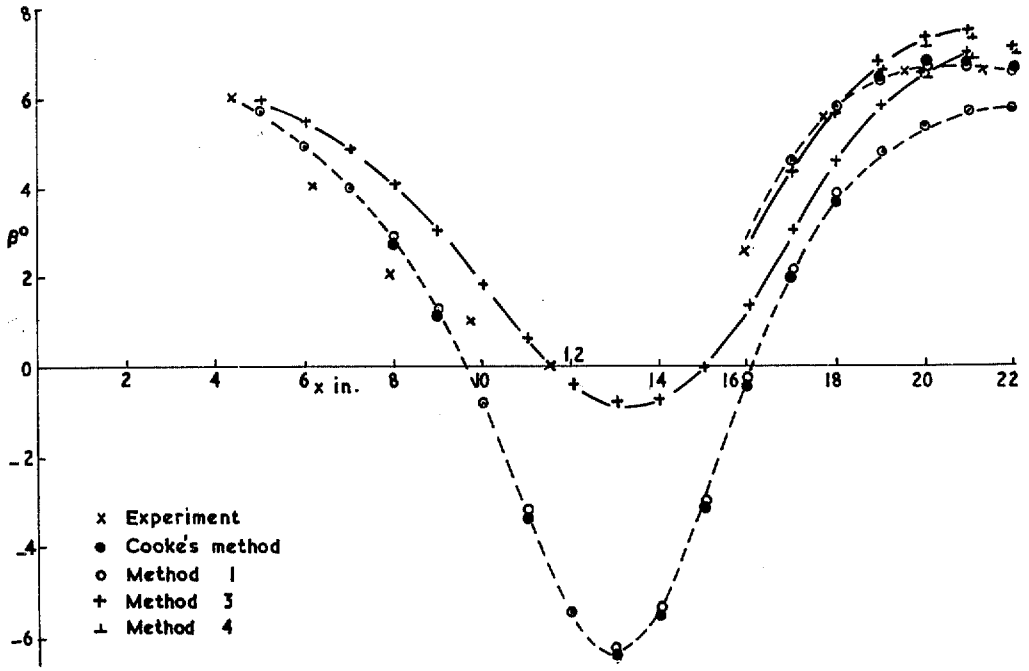

FIG. 14. Angle between limiting and external streamlines plotted against distance normal to the leading edge. Run 4.

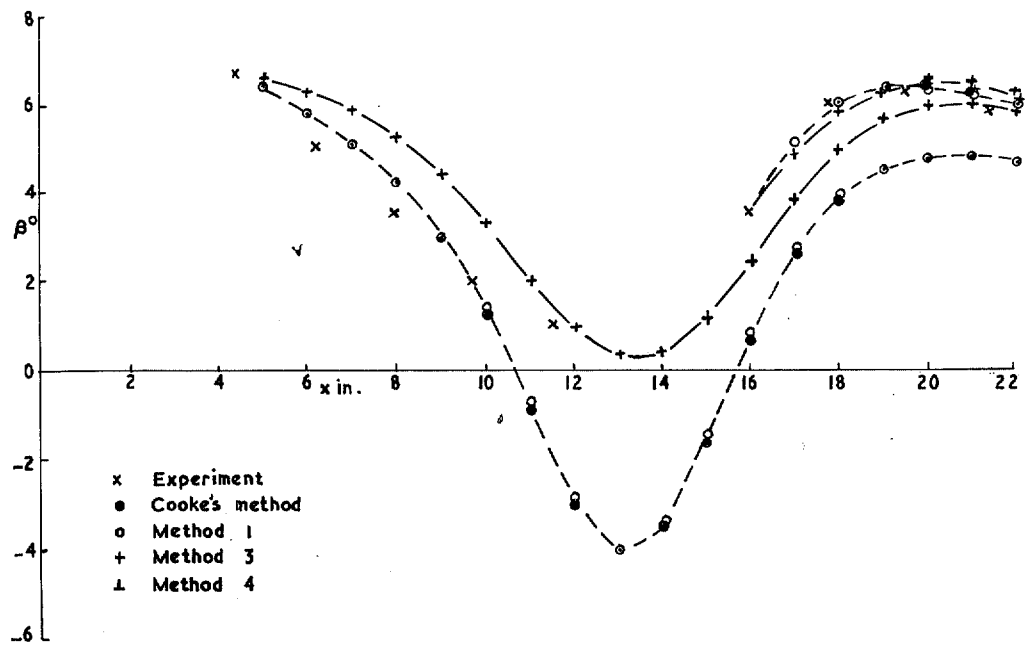

FIG. 15. Angle between limiting and external streamlines plotted against distance normal to the leading edge. Run 5.

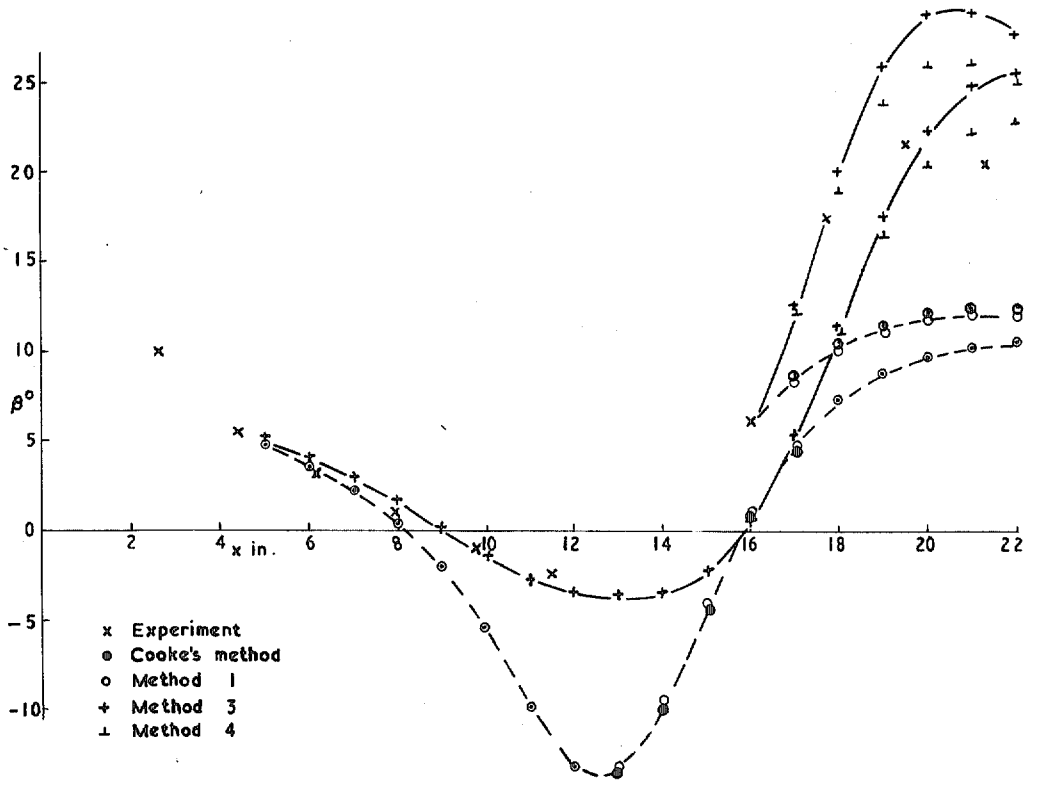

FIG. 16. Angle between limiting and external streamlines plotted against distance normal to the leading edge. Run 6.

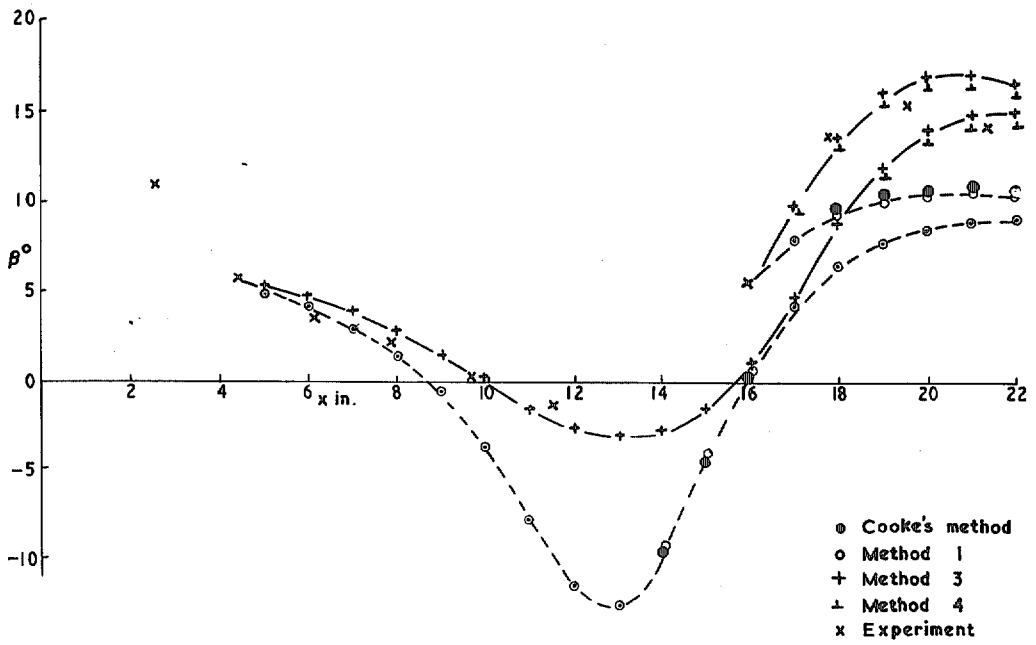

FIG. 17. Angle between limiting and external streamlines plotted against distance normal to the leading edge. Run 7.

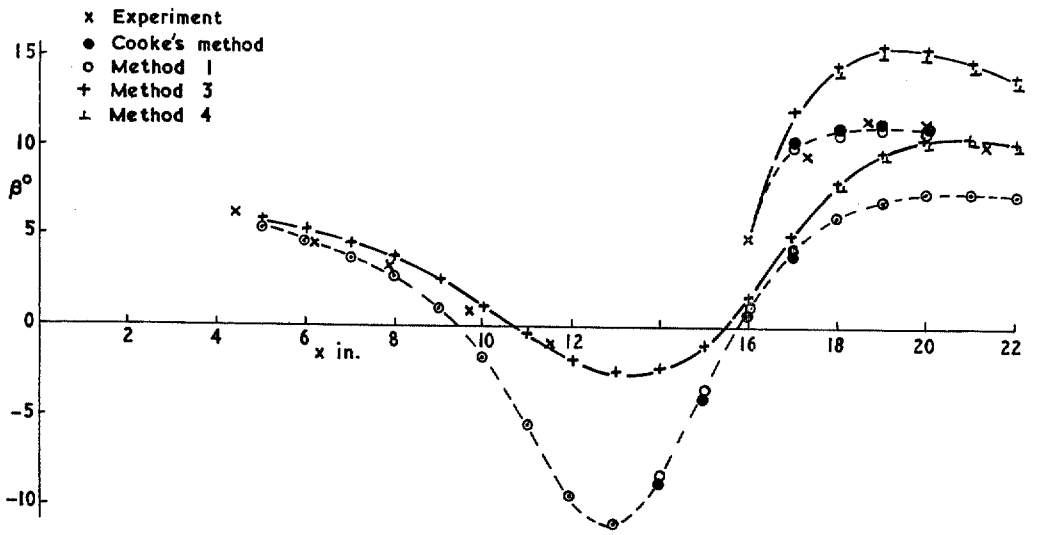

FIG. 18. Angle between limiting and external streamlines plotted against distance normal to the leading edge. Run 8.

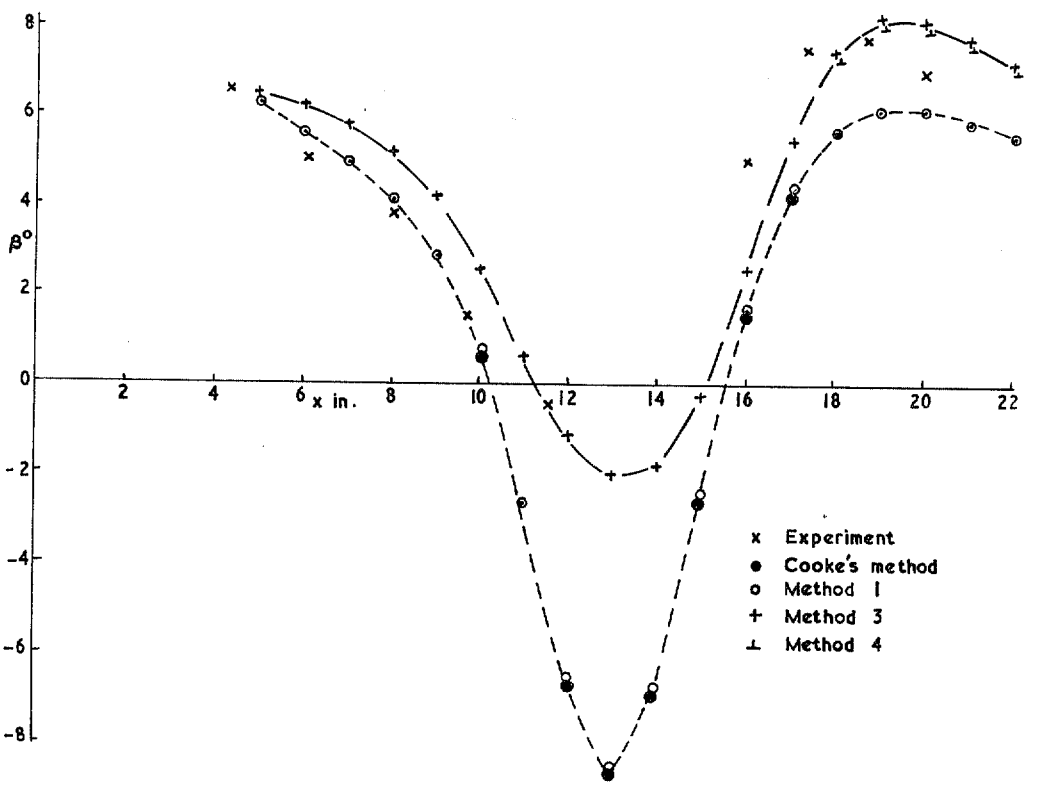

FIG. 19. Angle between limiting and external streamlines plotted against distance normal to the leading edge. Run 9.

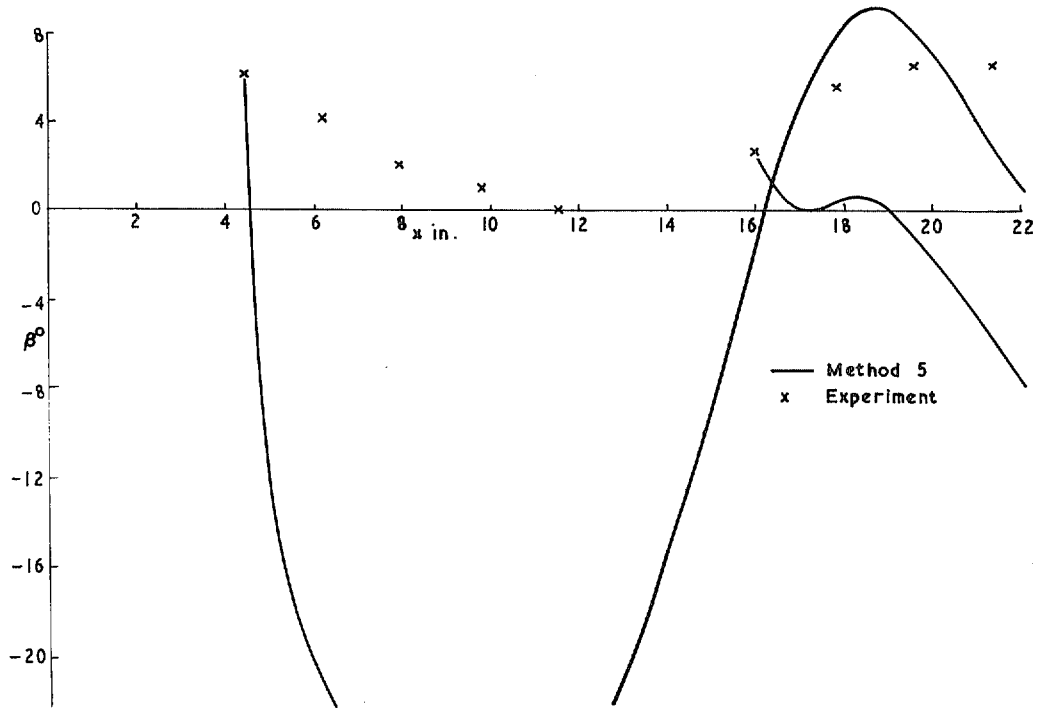

FIG. 20. Angle between limiting and external streamlines plotted against distance normal to the leading edge. Run 4.

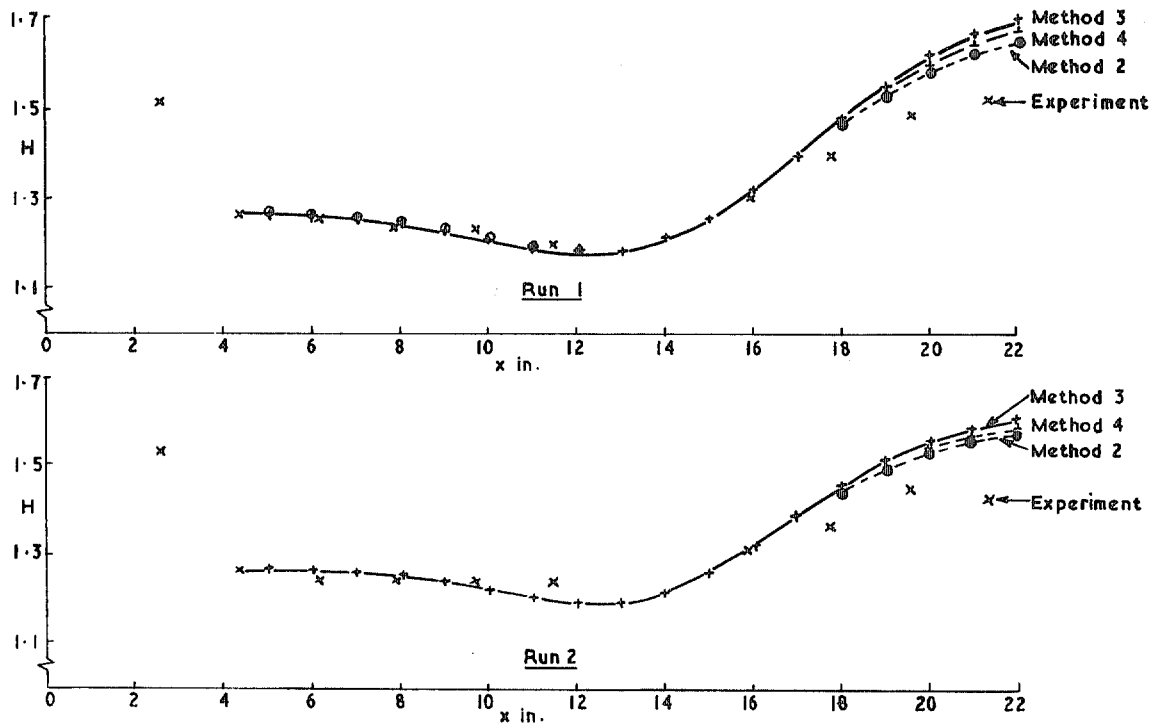

FIG. 21. Streamwise shape factor plotted against distance normal to the leading edge.

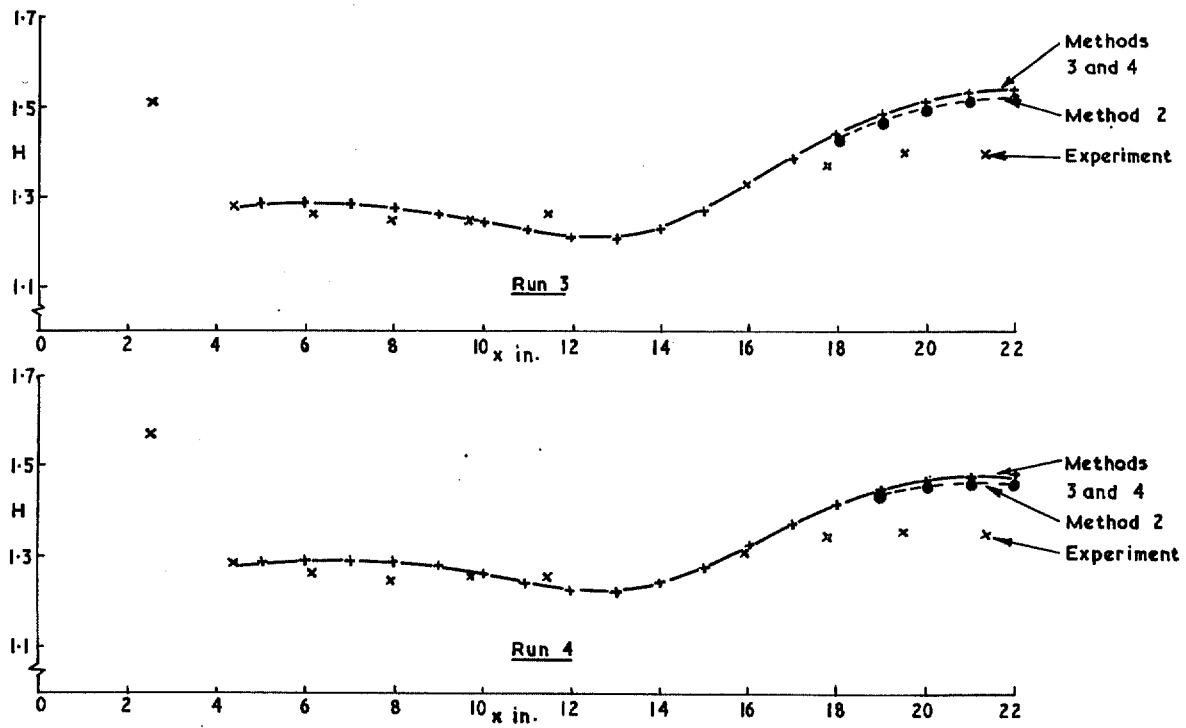

FIG. 22. Streamwise shape factor plotted against distance normal to the leading edge.

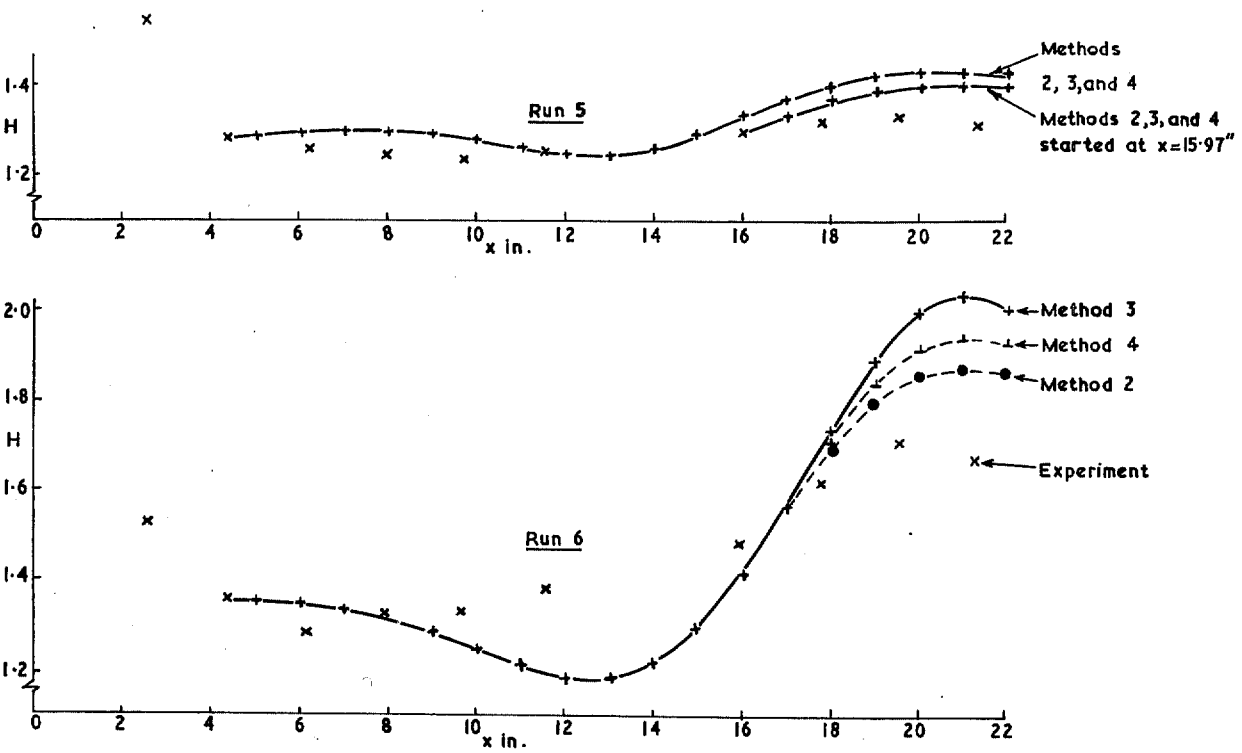

FIG. 23. Streamwise shape factor plotted against distance normal to the leading edge.

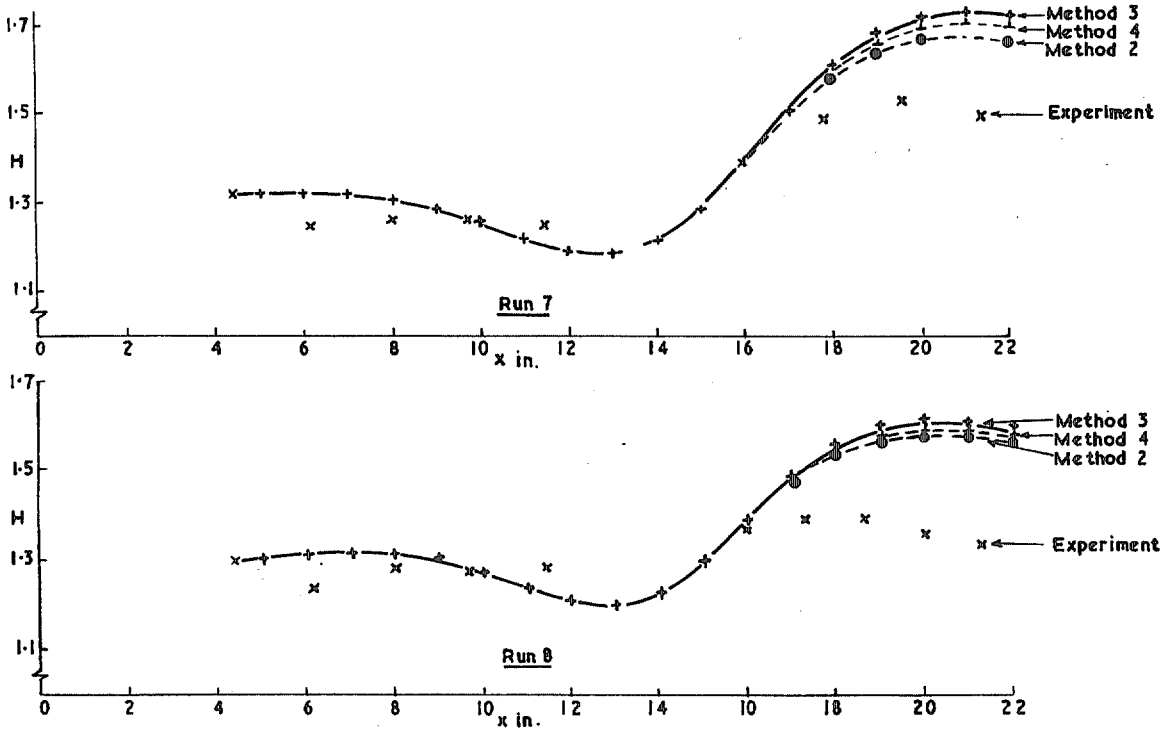

FIG. 24. Streamwise shape factor plotted against distance normal to the leading edge.

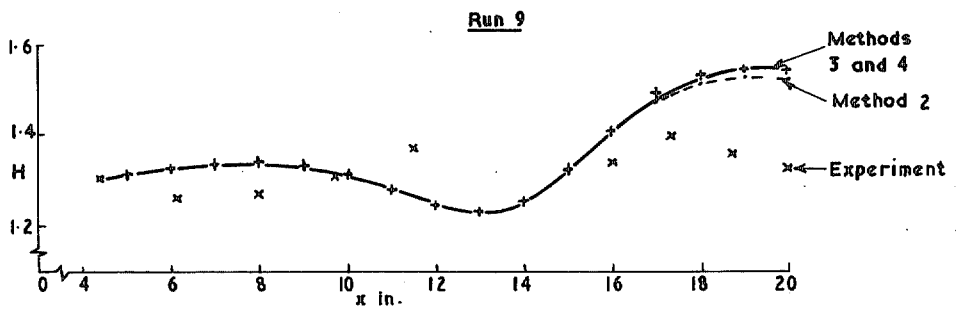

FIG. 25. Streamwise shape factor plotted against distance normal to the leading edge.

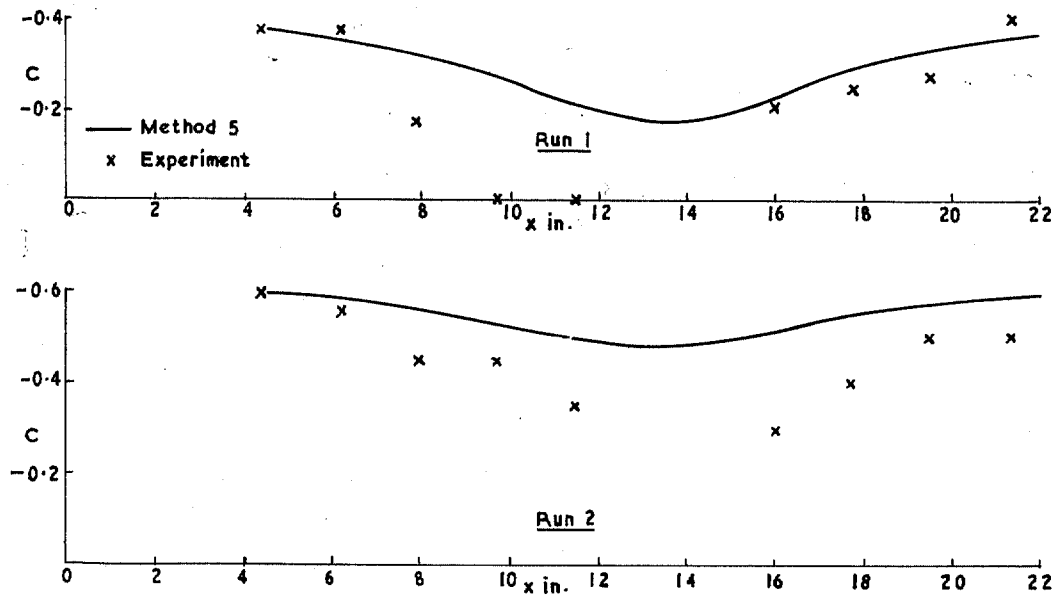

FIG. 26. Values of C where C = Limit $v/(u-u_e)$ plotted against distance normal to the leading edge. $u/u_e \to 1$

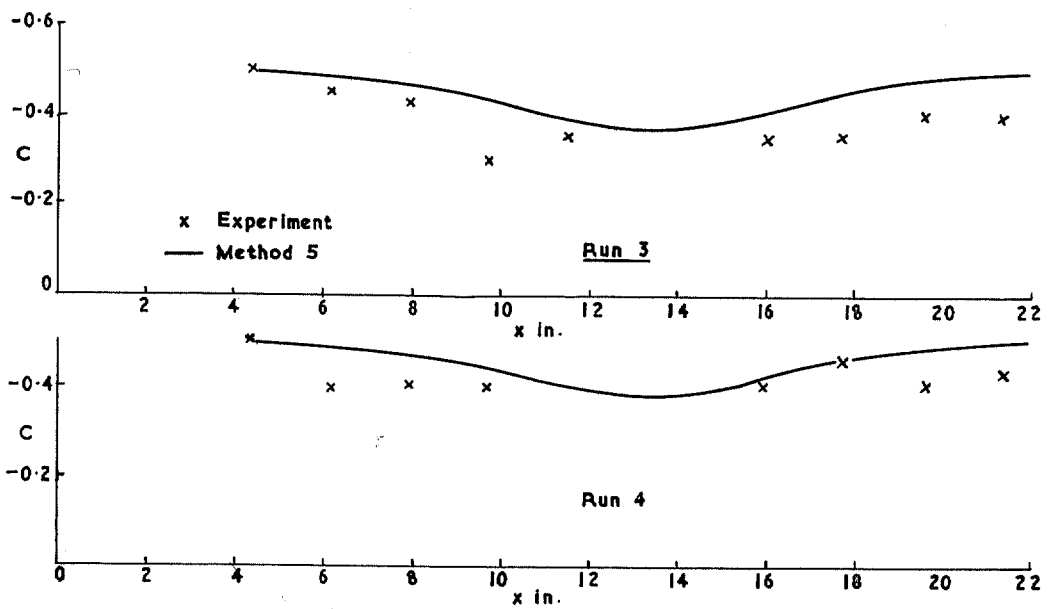

FIG. 27. Values of C where C = Limit $v/(u-u_e)$ plotted against distance normal to the leading edge. $u/u_e \to 1$

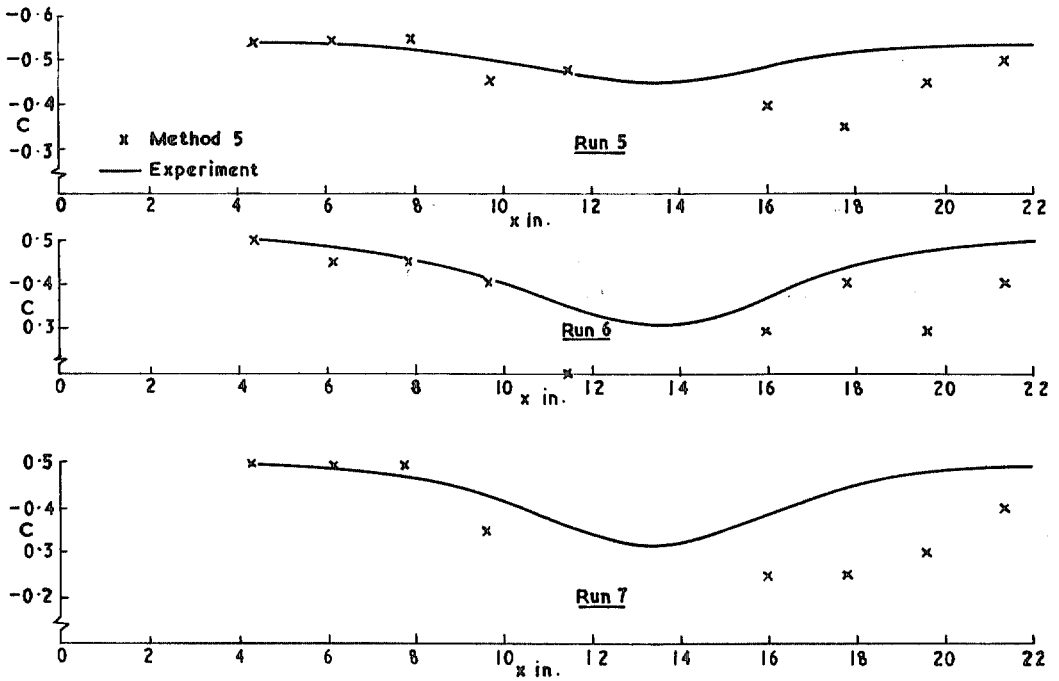

FIG. 28. Values of C where $C = \text{Limit } v/(u-u_e)$ plotted against distance normal to the leading edge. $u/u_e \to 1$

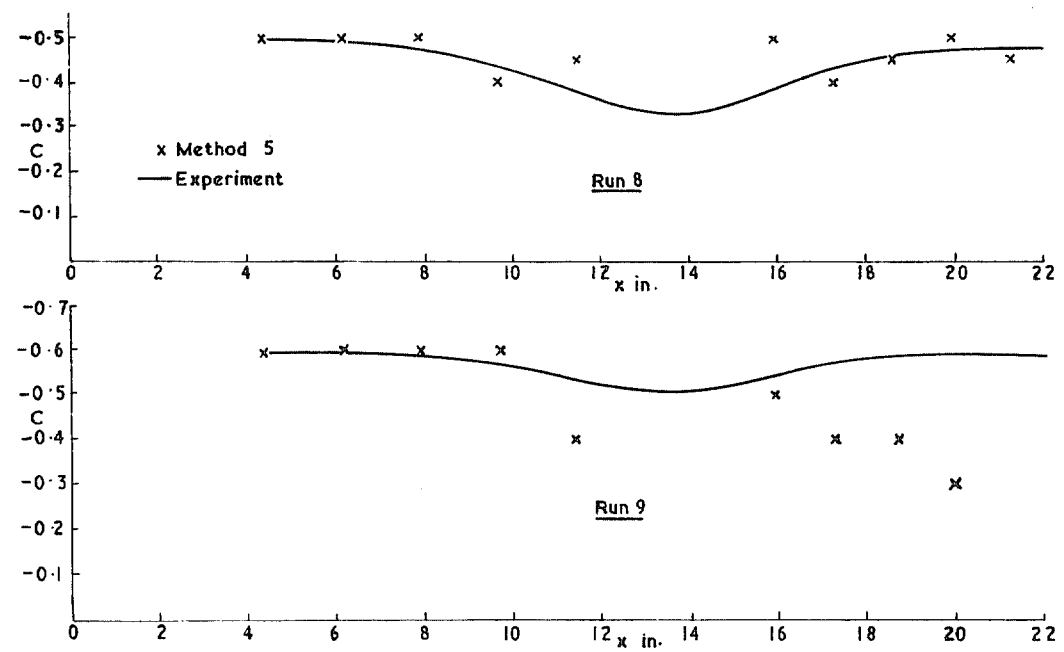

FIG. 29. Values of C where $C = \text{Limit } v/(u-u_e)$ plotted against distance normal to the leading edge. $u/u_e \to 1$

Printed in Wales for Her Majesty's Stationery Office by Allens Printers (Wales) Limited

Dd.129527 K5

Published by
HER MAJESTY'S STATIONERY OFFICE

To be purchased from
49 High Holborn, London W.C.1
423 Oxford Street, London W.1
13A Castle Street, Edinburgh 2
109 St Mary Street, Cardiff CF1 1JW
Brazennose Street, Manchester 2
50 Fairfax Street, Bristol 1
258–259 Broad Street, Birmingham 1
7–11 Linenhall Street, Belfast BT2 8AY
or through any bookseller

S.O. Code No. 23-35